We are IntechOpen, the world's leading publisher of Open Access books Built by scientists, for scientists

4,800
Open access books available

122,000
International authors and editors

135M
Downloads

Our authors are among the

154
Countries delivered to

TOP 1%
most cited scientists

12.2%
Contributors from top 500 universities

CLARIVATE ANALYTICS BOOK CITATION INDEX INDEXED

WEB OF SCIENCE™

Selection of our books indexed in the Book Citation Index in Web of Science™ Core Collection (BKCI)

Interested in publishing with us?
Contact book.department@intechopen.com

Numbers displayed above are based on latest data collected.
For more information visit www.intechopen.com

10

Detection of Carbon Nanotubes Using Tip- Enhanced Raman Spectroscopy

Jia Wang, Xiaobin Wu, Rui Wang and Mingqian Zhang
State Key Laboratory of Precision Measurement Technology and Instruments, Department of Precision Instruments, Tsinghua University, Beijing China

1. Introduction

As a kind of new nano-materials, carbon nanotubes (CNTs) are of the particular properties, in the aspects of physics, mechanics, electronics, optics and so on. They indicate the remarkable potential applications in the nano-electronic devices, composite materials, scanning probe microscopy (SPM), field emission, hydrogen storage and environment protection. The research on CNTs has become a hot spot in the fields of nano-science and nano-technology, especially in nano-materials (Iijima, 1991; Yu et al., 2000; Frank et al., 1998; Chiang et al., 2001).

The commonly used methods for the measurement and characterization of CNTs include the scanning electron microscopy (SEM), transmission electron microscopy (TEM), scanning probe microscopy (SPM), Raman spectroscopy, infrared spectroscopy and so on. Electron microscopy and SPM are commonly used in nowadays research on nano-science. And both of them provide direct characterization of the topography and nano-structure of CNTs with comparatively high spatial resolution. However, they fail to provide the corresponding specimens' chemical information, which is also required in the research and identifications of nano-materials and nano-structures.

Raman spectroscopy is one of the spectral analysis methods used to detect vibrational, rotational, and other low-frequency modes information of the specimen structures or molecular structures, and is usually employed to obtain the structural information of CNTs (Rao et al., 1997; Dresselhaus et al., 2002; Dresselhaus et al., 2005). However, this spectral method is subject to two obstacles. One is the diffraction-limited spatial resolution, and the other is its inherent small Raman cross section and weak signal.

As facing the challenges of nano-scale measurement, a new characterization method, which can simultaneously obtain topography characteristics with nanometer resolution and spectral information from nanometer localized specimen surface is desiderated.

Tip-Enhanced Raman Spectroscopy (TERS) is an emerging technology developed to realize the aim mentioned above in the recent years (Stöckle et al, 2000; Hayazawa et al., 2000; Hartschuh et al., 2003; Pettinger et al., 2004). It spans the main obstacles of conventional Raman spectroscopy by tactfully combining the near-field optics advantage of nanometric spatial resolution and spectroscopy of obtaining chemical information. Also the Raman signal from nanometer localized specimen surface is considerably enhanced with the tip-enhanced optical technology (TEOT) and the signal-to-noise ratio (SNR) is consequently

improved. Especially, in TERS, the topography and spectral information are obtained simultaneously. By correspondingly analyzing the two images, the specific recognition of the feature distribution can be realized.

With the development in recent years, TERS has been applied to the characterization of nano-materials(Hayazawa et al, 2003; Huihong et al., 2006; Hartschuh et al., 2003), biological specimens(Anderson et al., 2003; Watanabe et al., 2004; Bailo & Deckert, 2008), dye molecules(Hayazawa et al., 2000; Pettinger et al., 2004; Watanabe et al., 2005), and semiconductor materials (Sun et al., 2003; Lee et al., 2007; Saito et al., 2008; Sun & Shen, 2001). In January 2008, the topic meeting, entitled as "Tip Enhanced Raman and Fluorescence Spectroscopy (TERFS): Challenges and Opportunities", was held in the National Physical Laboratory (NPL), London, Britain. Over a hundred of scientists and scholars from eleven countries and a number of equipment manufacturers attended this meeting. Research results and experiences were shared and the challenges and prospects of TERS were discussed. TERS has been demonstrated as a promising tool in the characterization of nano-materials and nano-structures, and provides powerful approach for the research of nano-science. It surely has the potential to expand the knowledge and comprehension of the phenomena and laws in the nano-scale.

However, the technique challenges involved in TERS system is more complicated than the SPM setup or the Raman spectroscope individually. At present, several companies can provide the commercial TERS system. Yet, as an emerging spectral analysis approach TERS is still in the developing process, and the integrated commercial systems are often difficult to adapt to the rapidly boosting research and detection needs in different fields. The thorough understanding of the TERS principle and key technologies is very beneficial whether to master the operation of commercial systems, or to buildup their own TERS systems upon specific detection needs.

In this chapter, TERS Measuring principle and system are firstly introduced and some key techniques are discussed in section two. CNT specimen preparation is introduced in section three. Carbon nanotube, single-walled carbon nanotube (SWNT) and multi-walled carbon nanotube (MWNT) specimens are detected by the TERS and results are discussed in section four. Some conclusions are presented and future works are discussed in the CNT detection using TERS in the section five.

2. TERS measuring system

Combining a SPM and Raman spectroscopy, TERS is of the ability to simultaneously obtain topography and corresponding spectral information of the specimen with high spatial resolution and high sensitivity. It provides powerful and promising tool for the characterization and research of nano-scale materials. The TERS systems are generally composed of the SPMs, the illumination/collection configurations and the Raman spectroscope. In this section, TERS's working principle, measuring system and some key techniques will be introduced and discussed.

2.1 Principle of TERS

Raman spectroscopy is one of the common spectral analysis methods used to detect molecular vibration, rotation, other low-frequency modes and chemical information of specimen and is usually employed to obtain the structure and vibration information of CNTs (Rao et al., 1997; Dresselhaus et al., 2002; Dresselhaus et al., 2005).

Two obstacles have to be faced when try to use conventional Raman spectroscopy to characterize CNTs. Firstly, the resolution of conventional Raman spectroscopy is limited by the optical diffraction limit to about half-wavelength. It corresponds to an zone of about 200×200 nm. Thus, the conventional Raman spectroscopy can only obtain the average spectral information of the chemical composition from the whole illuminated area of the nanometer specimen. Meanwhile the measurement and characterization of basic nano-element and nano-composition is vital in nano-material research. Secondly, another difficulty is the low detection sensitivity as nanometer localized spectroscopy is detected. Since the cross section of Raman scattering is quite small, the spectral signal is too weak to be directly detected. Additionally, the quantity of sample in nano-materials research is rather limited. It consequently results in the extremely weak response signal even using a strong exciting illumination beam. Thus, according to the conventional approach, the spectral detection requires long acquisition time and only obtains poor signal-to-noise ratio result. It is crucial to efficiently enhance the optical signal to obtain desirable sensitivity and SNR.

In sum, characterization of CNTs faces the major challenges with the Raman spectral approach are to obtain a high-resolution beyond the diffraction limit localized spectral signal with sufficient sensitivity and corresponding topography information in nanometer scale of the specimen.

As shown in Fig.1, the incident beam with appropriate wavelength and polarization state is focused at the apex of the nano-scale metallic tip. Excited by the incident laser, an enhanced electric field is generated in the vicinity of a metallic tip. The mechanism of the enhancement can be attributed to the localized surface plasmon resonance (LSPR) effect (Bohren & Huffman, 1998) and the lightning-rod effect (Novotny et al., 1997). The metallic tip can be regarded as a nano-scale light source with quite high power density. Consequently, Raman signal from the localized position of the specimen excited by the enhanced field very close to the tip is markedly enhanced. Since the enhancement of the Raman intensity is proportional to the 4th power of the electric field enhancement (Kerker et al., 1980), the Raman signal enhancement obtained in TERS experiment is usually up to 10^3~10^6. The enhanced spectral signal is scattered and converted into the far-field by the tip. Through the collection optics, the Raman signal is guided into the Raman spectroscope to be further analyzed.

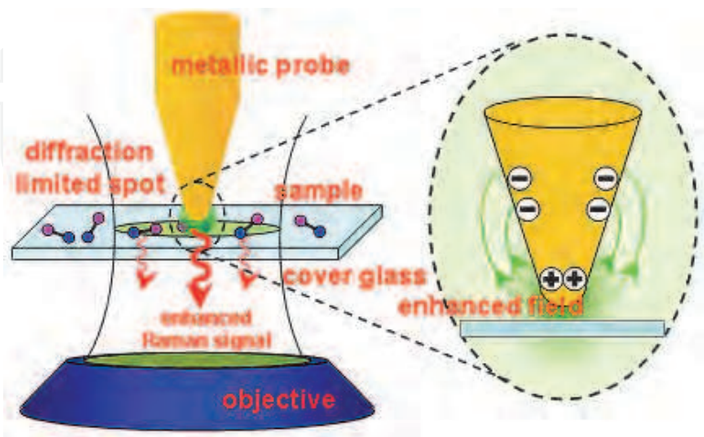

Fig. 1. Concept of tip-enhanced Raman spectroscopy (TERS) shows a strongly enhanced optical field generated at the apex of sharp metal tip of SPM by the external illumination (R. Wang, 2010c).

By means of scanning the tip over the specimen at a certain distance, tens nanometers above the surface, the corresponding topography and Raman information from specimen can be obtained simultaneously.

TERS is a skillful combination of the SPM (or SNOM) and Raman spectroscopy, and an improved variant of the surface enhanced Raman spectroscopy (SERS). It may be imagined that the rough metallic surface excited and enhanced in SERS is scaled down to a nanometer "hot-spot" scattering Raman spectral signal enhanced from the tip apex (Otto, 2002). In this situation, the distance and relative position between the "hot-spot" and the specimen is precisely controllable. Thus, the irksome measurement uncertainty and non-repeatability in the former SERS detection caused by the random distributed enhancing "hot-spots" on the rough metal substrate is avoided. Overall, the single effectively enhancing "hot-spot" of TERS provides an access to the repeatable characterization and quantitative analysis of the low density CNTs content specimen. Additionally, it provides a better understanding of the enhancement mechanism. TERS not only has the nanometer spatial resolution, but also has Raman spectral analysis performance.

The efficient excitation of electromagnetic-field enhancement requires the incident light to match with surface plasmon wave vector. To satisfy this condition, some factors of the enhancing system should be taken into consideration, including metal materials, size, tip shape, excitation wavelength, beam polarization state, and incident angle and surrounding refractive index (Martin & Girard, 1997; Krug et al., 2002; Neacsu et al., 2005). As theoretically predicted and experimentally proved, gold and silver are most suitable materials for generating enhancement under visible light illumination. Furthermore, according to the lightning-rod effect, the most contribution to the local field enhancement owes to the longitudinal electric components which polarization is along the axis of the tip rather than the horizontal E-components perpendicular to the axis of the tip. Therefore, in order to obtain effective enhancement, it is ideal to use a longitudinal E-component to excite at the tip apex.

2.2 System of TERS

As shown in Fig.2, a typical TERS system consists of a SPM, illumination/collection optics and a Raman spectroscope and other mechanical, optical and electronic devices in an integrated detection system. The separation between the tip and the specimen is regulated and as well as kept in few to tens nanometers during the scanning detection. The illumination optics focuses the incident light on the tip apex to excite the enhanced local field and Raman signal. The localized spectral signal is scattered and converted by the tip apex and then collected with the collecting optics in the far-field. In fact, the obtained signal is mixture that includes the tip-enhanced near-field Raman signal and the far-field background signal. Then, all of collected Raman signal are guided to the spectroscope to be analyzed. In TERS, the far-field Raman signal is regarded as the background noise, because it contains the spectral information of the whole illuminated area rather than only the nanometer zone beneath the tip. A common method to deduct the far-field background is to withdraw the tip from the focus to detect the far-field Raman signal and subtract it from the mixture signal. The fundamental of TERS system design is to raise the efficiency of signal excitation, collection and improve the SNR, that is, to increase the near-field signals while suppress the background noise. By means of point-by-point scanning the tip over the specimen, the corresponding topography and Raman signal of the specimen can be obtained simultaneously.

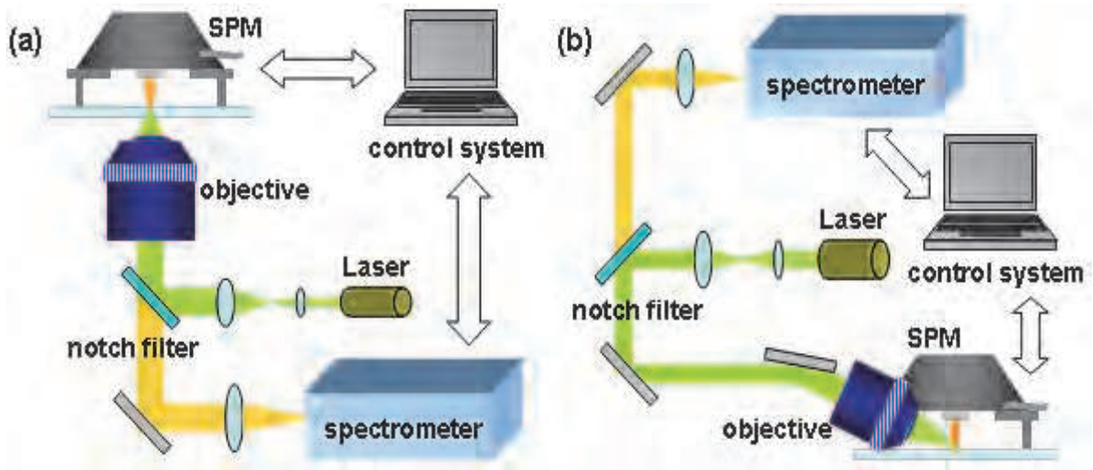

Fig. 2. Schematic diagrams of TERS systems in transmission mode (a) and in reflection mode (b).

2.2.1 Illumination/collection configurations

According to the illumination/collection configurations, TERS systems can be divided into transmission-mode ones and reflection-mode ones.

Considering the structural and spatial constrains, the illumination and collection configurations often shares the same one-objective-lens-based optical path. The configuration of the transmission-mode TERS system usually employs an inverted microscope. The incident laser is tightly focused with a high numerical aperture (N.A.) objective on the tip apex and the backward-scattered tip-enhanced Raman scattering signal is collected with the same objective. The transmission-mode TERS is of ability to reduce the far-field background signal with a high N.A. objective and the SNR is considerably improved and the system construction is relatively simple. Nevertheless, the applicability of transmission-mode TERS is restricted. It can only be suitable to detect transparent or sparsely distributed specimens.

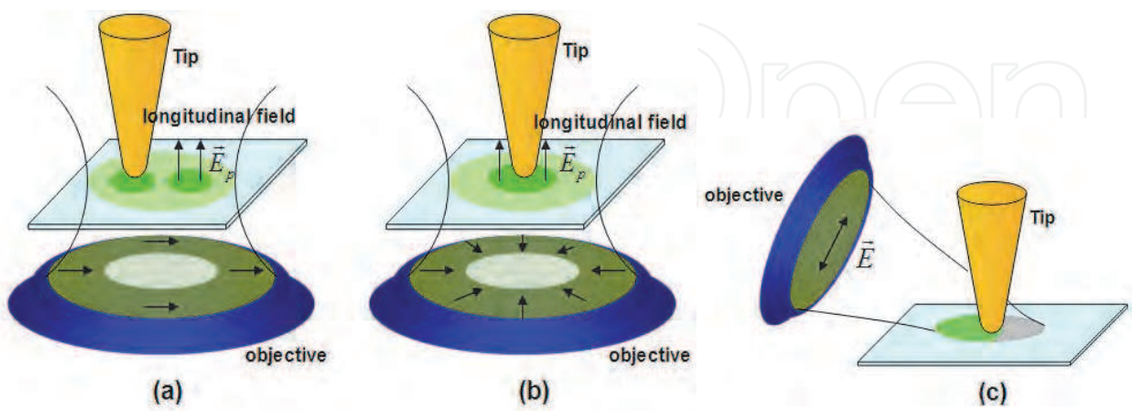

Fig. 3. Schematic diagrams of tip-enhanced Raman spectroscopy using (a) linearly polarized light (or beam) annular illumination; (b) radially polarized annular illumination; (c) linearly polarized side illumination.

The reflection-mode TERS systems are suitable for detecting any specimens regardless of the transparency. This kind of systems often utilizes a side-illumination/collection configuration (Fig. 3(c)). The incident light pass through a long working distance objective located at the side of the SPM scanning head and is focused on the tip apex. In this configuration, only the long working distance objective with lower N.A. (NA<0.6) can be used. The not-so-tightly focused laser oblique incident on the specimen surface and illuminate a relatively large elliptical area. The undesirable increased illuminated area leads to stronger far-field background noise. Therefore, the side-illumination reflection-mode TERS suffers from the lower SNR and signal collection efficiency.
One of illumination problems is how to generate the strongest longitudinal electric components to excite the most efficiently the field enhancement close to the tip. One of the solutions is to choose appropriate polarization light as the exciting beam (Hayazawa et al., 2004; Saito et al., 2005; Anderson et al., 2006). The possible choices include linear polarization, circular polarization, radial polarization and azimuthal polarization light. It will be discussed in detail in the following section.

2.2.2 Distance control and topography measurement

Intend to enhance the localized Raman signal and obtain high resolution near-field optical information, a sharp metallic tip is precisely located in the near-field region of the sample under test and controlled at a certain few nanometers' distance from the sample surface. Generally, the distance is maintained within 10 nm. In TERS system, the SPM technology is employed to control the tip-specimen separation. During the scanning detection, the constant separation is maintained by the feedback control from SPM. Furthermore, the height of the specimen surface is measured and consequently the topography data can be obtained.
Generally, there are three types of SPMs often used as components to build up TERS systems: scanning tunneling microscope (STM), atomic force microscope (AFM), and shear-force microscope (SFM).

2.3 Key technology in TERS system

Typical TERS system combines the SPM, illumination/collection optics, Raman spectroscope with other mechanical, optical and electronic devices. There are certain key technologies involved in this integrated detection system, including the fabrication of TERS tips, selection of SPM, dual scanner/dual closed-loop controller, illumination with radially polarized beam, illumination/collection configuration based on parabolic mirror, characterizing optical properties of the tips with white light, and substrates.

2.3.1 Fabrication of TERS tips

It is indubitable that the tip is the most crucial element in TERS deciding both spatial resolution and Raman enhancement efficiency.
The most suitable metal materials for tip are silver and gold, which are proven theoretically and experimentally for TERS systems. They both can provide most effective tip-enhancement under visible light illumination. Silver is capable of providing stronger enhancement, because its imaginary part of permittivity is smaller (Johnson & Christy, 1972). However, since the Ag tips are rapidly oxidized in air, they need to be protected properly and used timely. On the other hand, gold tips are chemically inert against oxygen and stable against radicals.

The fabrication of metal-coated AFM tips used in TERS system (AFM-TERS tips) is often based on the commercial Si or Si3N4 AFM tips. And the physical coating method (evaporation, deposition, or sputtering) is utilized to metallize the AFM tip. It is need to note that the stress of the metal coating might bring in the warping problem of the AFM cantilever and affect the performance of the tip. Typically, the TERS tips acquired via this method are unlikely to provide significant enhancement and are frequently being scraped during scanning (Kharintsev et al., 2007).

The coating of the AFM tip can also be realized via chemical approach such as silver mirror reaction (Saito et al., 2002; J. J. Wang et al., 2005). However, the reactants may contaminate the cantilever and worse, yet still attach to the tip apex. Another issue concerning AFM-TERS tips is that the Raman signal of the inner material of the TERS tips (Si or Si3N4) is also being enhanced and exists as the noise. Especially in the research on semi-conductor materials, this issue should be pay closer attention to (Lee et al., 2007).

The preparation of STM-TERS tips is comparatively mature. The tips are fabricated from high purity single-crystal gold (Ren et al., 2004) or silver wires. The metal wires are shaped with electrochemistry etching. This method is capable of providing gold STM-TERS tips with effective enhancement and small tip apex size. And the success rate (tolerant) is high. However, it is not so good to fabricate silver wire tip (Pettinger et al., 2002).

The preparation method of SFM-TERS tips is more flexible. Addition to the previously mentioned etched gold tips (Hartschuh & Novotny, 2002), the etched tungsten tips with gold or silver coating (Sun & Shen, 2001), are also suitable to the SFM in TERS system. In recent years, the method demonstrates obvious advantage of attaching gold or silver nano-particles to the apex of the fiber probe (Kalkbrenner et al., 2001). By optionally selecting the size of the nano-particles, the optical property of the TERS tip can be designed to obtain strong Raman enhancement. In addition, since the refractive index of fiber is lower, far-field Raman scattering enhanced causes by the body of the tip can be effectively suppressed.

In addition to these mentioned methods above, in order to achieve precise control of the size and structure of the tip for improving the enhancement efficiency, focused ion beam etching (FIB) has been used to produce TERS tip (Frey et al., 2002). But since the FIB processing is complex and costly, it has not being widely used.

2.3.2 Selection of SPM

As shown in Fig.4, STM, AFM, and SFM are the three types of SPMs commonly used as components to build up TERS systems. They have different feedback mechanisms and respective technique features. Although, they are all able to regulate effectively the tip-specimen separation and obtain the topography. The TERS systems based on the different types are of the different technical properties. Therefore, the TERS systems based on appropriate SPM components can be selected in dependence to the sample and experimental condition. The performance properties of the STM, AFM, or SFM in TERS systems are list in Table 1.

2.3.3 Dual scanner/ dual closed-loop controller

Different from common SPMs, our homemade TERS system has a configuration of dual-scanner/dual closed-loop controller in which the two scanners and two closed-loop controllers are able to work independently.

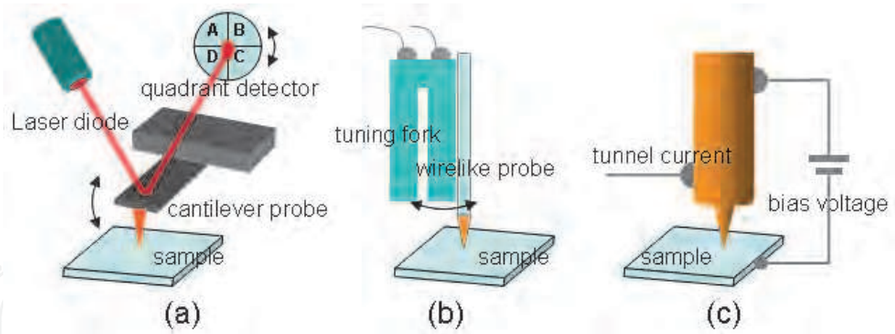

Fig. 4. The SPM equipment for TERS: (a) Atom force microscope; (b) Shear-force microscope; and (c) Scanning tunnel microscope. (R. Wang, 2010c)

SPM	Feedback types	Advantages	Disadvantages
AFM	Optical lever feedback	1) without limit to sample types and environment; 2) easy to operate, convenient to be combined with other AFM imaging methods; 3) able to study pressure-induced spectral changes by tip (Watanabe et al.,2004; Saito et al.,2008).	1) easy to damage metallic coating of tip; 2) low-enhancement factor; 3) stray light from optical lever interferes spectral measurement.
SFM	Tuning fork/Shear force feedback	1) without limit to sample types and environment, little damage on samples, especially for biological sample in liquid; 2) easy to fabricate tip; 3) convenient to be combined with inverted and upright microscope respectively.	1) complicated operation; 2) poor lateral resolution.
STM	Tunneling current feedback	1) high spatial resolution and high control precision; 2) working in gap mode with high detection sensitivity and high-resolution spectral imaging; 3) mature fabricating technique to produce tips.	1) only conducting samples or ultra-thin samples distributed on conducting substrate; 2) mostly working in reflection mode due to opacity of sample or substrate. 3) surface undulation of sample no more than a few hundred nanometers usually

Table 1. Comparisons of TERS systems based on AFM, SFM and STM

2.3.3.1 Dual scanner

The scanning types of SPM can be divided into two types, sample stage scanning and tip head scanning. For the former type SPM, a scanning stage on which the sample is attached to is driven by the scanner and moves in a raster pattern below the tip. The tip only moves along its axis to adjust the tip-specimen separation. For latter type SPM, the tip is always amounted on a 3-D movable scanning head, and the sample is kept still. The progressive scanning and the tip-specimen separation are both controlled by the tip scanning controller. Conventional SPM usually works with one controller in one particular mode. However, SNOM and TERS systems work more complexly than the conventional ones. For SNOM or TERS detection, it needs to appropriately couple the incident light beam to illuminate and excite the sample in a certain condition\manner, which may relate to wavelength, incident angle, focused beam, specific polarization. Additionally, appropriate optical configuration for collecting the scattering, transmission, or reflection light in 3-D space or a specific direction is also required.

However, it is difficult to meet various kinds of detection demands to the diversity of specimens with single scanning type systems. For example, if the CNTs specimen is put on the sample stage, and the optical axis of the illumination configuration is coaxial with the tip axis, stage scanning mode is then appropriate for the optical alignment principle. But in other conditions the tip scanning is requested, such as detecting the SPP waveguide which needs to be precisely coupled with external fixed optical path for excitation and collection. Although the tip might be possible to slightly deviate from the optical axis during the scanning, the impact of the nanometer deviation can be negligible.

Therefore, it is preferable to employ the dual-scanner configuration which can provide the sample stage scanning and the tip head scanning in TERS system respectively. Its advantages include more precise control, arbitrarily choosing sample, and scanning mode to any different requirements of sample detection, illumination alignment, or optical coupling mode. It is convenient to tip-illumination alignment and ensures the optimal detection results.

The common requirements to the dual-scanner configuration:

a. Accurate, real-time, and closed-loop measuring/ to control the tip-sample separation;
b. Precise alignment of the tip apex with the excitation focus;
c. Nanometer accuracy, high repeatability, point-by-point scanning in raster mode over the whole detected region to obtain the sample information.

2.3.3.2 Dual closed-loop controller

In order to ensure two independent scanners to work with high-precision positioning and high repeatability two independent closed-loop controllers should be equipped in a TERS system. Nanometer accurate positioning and scanning are usually realized with a piezoelectric actuator. The measuring time for TERS is usually much longer than SNOM imaging and in result the higher stability and repeatability are required in the TERS system.

Firstly, the piezoelectric scanner might drift a certain distance with ambient temperature fluctuation. Thus, the real-time closed-loop control is required to correct and eliminate the impact of drifting, and improve the accuracy and repeatability. It is of significant importance to collecting, processing, and analyzing the Raman information and the topography data correspondingly.

Another important issue to be considered is that the certain integration time is needed to each detected point to acquire Raman spectrum data in TERS detection. Since the Raman signal is extremely weak, even with the highest sensitivity spectral detector, it still needs to spend certain integration time. Meanwhile, the location and the topography data at the point are recorded. It is distinct from the regular SPMs scanning point-by-point and line-by-line with relative high frequency, the scanning speed of TERS detection is rather slow or even stops at each detected point. It is evident that to measure the topography and point-by-point spectra with TERS requires much longer detection time than the regular SPMs. Therefore, TERS system demands the higher stability and repeatability which facilitate the tip and sample maintaining the relative position during the detection process.

Popular commercial SPM systems are usually only equipped with a 3-D controller. At the mean time, it is capable of closed-loop to control only one of the two scanners, either the scanner of the tip or the scanner of the sample stage. But the other not-under-controlled scanners may drift or disturbed by the external environmental perturbations such as the mechanical vibration. These all lead to the spatial mismatch of the detected spectral data and morphology data or even drive the tip out of the detected region. It seriously affects the results of experiments and the corresponding identification upon the Raman mapping and the relative topography data.

Therefore, two independent controllers should be used to realize the closed-loop control of the tip scanning head and the sample stage scanning precisely and respectively in TERS systems. Under closed-loop control, the 3-D scanning and positioning with high accuracy and repeatability can be realized by the two scanners respectively, and the internal drift of the scanner and the external perturbations of the environment can be effectively reduced. It ensures the spectral detection, topography detection, and the spatial corresponding data collection of the Raman spectra and the topography of the CNTs and other specimens. It is quite benefit for the corresponding analysis of the TERS result to recognize and identify the molecular structure, chemical information and characteristics of the sample.

2.3.4 Illumination with radially polarized beam

As mentioned above, in the lighting-rod effect, as the incident optical beam with the electric component parallel to the tip axis illuminates on the tip, the charge is driven to the foremost of the tip and forms a large surface charge accumulation at the tip apex. It means that the efficient enhancement of the local electric field at the tip apex will arise with illumination by the longitudinal E-component or incident polarization parallel to the tip axis (Novotny et al., 1997). While the polarization of the incident beam is perpendicular to the tip axis, the tip apex remains uncharged. So it does not actively contribute to the local field enhancement , also it may bring in the background noise.

Therefore, in order to obtain effective enhancement, it is crucial to form a longitudinal (parallel to the tip axis) E-component to efficiently arise the lighting-rod effect at the tip apex. The E-field distribution at the focus is determined by both the incident beam polarization and the optical configuration. It is crucial to make them to match to each other in the experimental setup.

How to generate experimentally a longitudinal E-component parallel to the tip axis?

In side-illumination situation, a linear polarization beam in TM mode illuminates the sample in a large incident angle. The most of the E-component of the incident optical field can be oriented parallel to the tip axis. And the strong longitudinal field excites effectively the strong field enhancement based on the lighting-rod effect.

In transmission-mode TERS systems, the incident beam is focused with high N.A. objective lens from the bottom to the tip apex as shown in Fig.3 (a) and (b). As the beam is linearly polarized (e.g. along x-axis), the distribution of the longitudinal field presents as two symmetric side lobes while the center is almost zero at the focus is shown in Fig.5(b). The reason is that the phase of the longitudinal E-component is out in the focus. If the tip is positioned at the center, the near-field enhancement is inefficient and the far-field noise is introduced by the transverse field illumination. To improve the enhancement and decrease the background noise, the tip has to be adjusted to either of the side lobes in the side of the focal center.

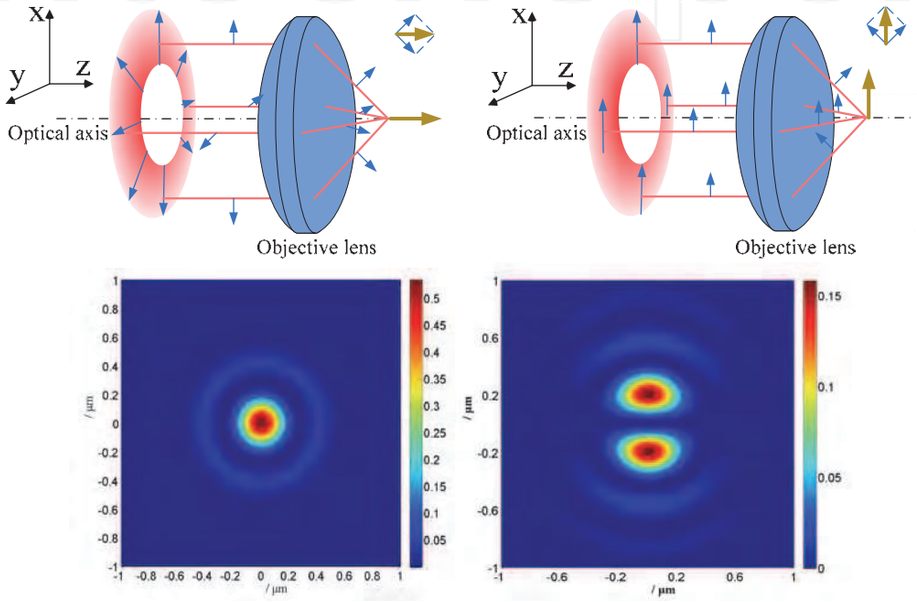

(a) (b)

Fig. 5. Longitudinal field distributions at the focuses of radial polarization (a) and linear polarization (b) beam focused by high N.A. objective.

Fortunately, a doughnut radially polarized incident beam focused by high N.A. objective is found to be more suitable in this kind of configurations. The first reason is that the longitudinal E-component is in-phase and causes enhancement at the focus as shown in Fig.5 (a). The second reason is that the symmetry of the doughnut radial polarization beam is more suitable to the axial or cylindrical symmetric optical system. No matter where one looks at, in any cross-section in the optical axis the field distribution is quite symmetric. The E-vector vibration directions of the radially symmetric rays are pointed against to each other. As focused by an objective at the focus with symmetrical incident angle, their E-vector vibration direction is in-phase in the longitudinal orientation and constructive interference. Especially when the radially polarized beam is tightly focused by a high N.A. objective, the stronger longitudinal field expected theoretically is effectively formed at the focus, Fig. 5(b). Therefore, the local enhancement can be actively excited by the longitudinal field as the tip entering the focus. Additionally, with radially polarized illumination, the longitudinal field area just locates at the center of the focus. It facilitates more convenient realization of optimal tip-longitudinal field alignment , coupling, efficient signal excitation and collection.

2.3.5 Illumination/collection configuration based on parabolic mirror

One of the significant advantages of reflection-mode TERS systems is that the detectable sample is not restricted no matter to transparency or opaque sample. This not only expands measuring range of specimens, but also allows more flexibility to the choice of substrates. The appropriate substrate can further promote the enhancement or reduce the background noise in TERS. But with side-illumination/collection configuration, only a long working distance objective with comparative low N.A. (typically smaller than 0.6) can be utilized. This results a strong far-field background noise and low collection efficiency.

Of late years, an illumination/collection configuration with a parabolic mirror (PM) has been introduced into the reflection-mode TERS system (Steidtner & Pettinger, 2007; Sackrow et al., 2008). This novel solution is considerable and promising in the research and industrial field of TERS.

The reflective surface of PM is shaped to an axial symmetric paraboloid. According to the geometric properties of the parabolic surface and the reflection law, the incident beam which is parallel to the axis of the PM is reflected by the reflector and converged to the focus of the parabolic surface. Instead of an objective lens, the PM converges the parallel incident light at the tip apex, and the enhanced Raman signal is collected with the same PM (Fig. 6).

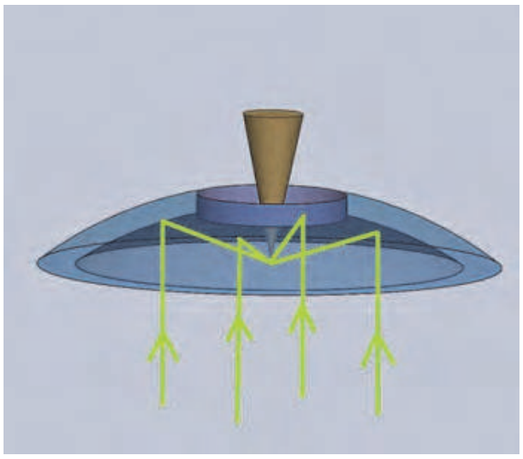

Fig. 6. Schematic diagrams of tip-enhanced Raman spectroscopy based on a parabolic mirror.

PM based reflection-mode TERS system has the following advantages:

a. In the PM based configuration, the focusing of the incident light is realized by reflection, instead of refraction in other objective lens based configurations. Because focusing with refection fundamentally avoid the chromatic aberration, regardless of the wavelength the incident parallel beam is focused at the fixed point. This facilitates the PM base TERS system, which can optionally employ different wavelength laser as excitation light (D. Zhang et al., 2009).
b. The N.A. of the PM used in this configuration can be up to approximately 1. With the high N.A. parabolic mirror, the incident light can be tightly focused at the tip apex to enhance the near-field Raman scattering. Still, the collection of the signal is also effective with the high N.A. parabolic mirror.
c. Unlike the side-collection one, the PM based configuration efficiently collects the signal from the whole 3-D space around the detected position.

d. The PM based TERS system works in reflection-mode, and neither the incident light nor the enhanced signal needs to transmit through the specimen. Therefore, it is capable of detecting any specimen regardless of the transparency or opaque.

It is also noticed that the optical system is cylindrically symmetric about the optical axis as well as the tip axis, like in the transmission-mode TERS. In order to generate a stronger longitudinal field at the focal region to excite the enhancement, a radially polarized donut-shaped incident beam should be utilized. Besides the more effective tip-enhancement result from the stronger longitudinal field, the far-field background noise is reduced simultaneously due to the smaller focal region.

But there are still several difficulties concerning the PM based TERS system. Firstly, this configuration requires the parabolic mirror with a higher precision surface shape. The PM which critically determines the illumination and collection efficiency is one of the most crucial components of the optics. In addition, the amount of far-field noise is related to the size of the focus, which depends on the shape of the reflector. Secondly, it is difficult to precisely align and couple the optical circuit. So it needs high skill and patience to adjust carefully.

2.3.6 Substrates

The TERS system rarely requires for the special preparation of the specimen or the specific experimental environment (air, liquid or vacuum). But it must be considered to reduce the far-field background noise and improve SNR. Yet, the highly dispersed thin film of specimen tends to demonstrate better TERS detection result. The choice of substrates on which the specimens dispersed is fairly tolerated.

Generally, the glass, mica, silicon or other commonly-used flat materials can all be utilized as the substrates in the TERS system based on AFM or SFM. In the STM based TERS system, single crystal metal or a metal coated surface is used. Numerous studies show that the material and microstructures of the substrate significantly affect the excitation of LSPs in the tip-specimen-substrate system. Considering that, only depending on the enhancement of the tip apex is hard to achieve the single molecule detection sensitivity and nano-meter spatial resolution, it would be ideal to further increase the enhancement factors and improving the confinement by appropriately bringing in the suitable substrate with nanometer structures.

In AFM or SFM based TERS system, using a SERS substrate can further enhance the Raman signal and quench the fluorescence. This technique is known as the SERS-TERS mode (Hayazawa et al., 2001). This kind of substrates can be prepared by depositing randomly distributed gold or silver nano-particles on the original substrate. As for STM based TERS system, the atomic-level smooth single-crystal gold surface is commonly used as the substrate. Under this composition namely gap-mode (Ren et al., 2005), an electromagnetic field enhancement can be greatly excited at the gap between the tip and the specimen.

Additionally, the smooth gold substrate eliminates the SERS enhancement induced with local surface fluctuations and provides an access to better understanding of the mechanism of the tip-enhancement effect.

2.4 Evaluation method of performances of TERS systems

Generally, there are 3 indicators used to evaluate the performance of a TERS system, including contrast, enhancement factor (EF), and the lateral resolution of the Raman mapping.

Contrast is defined as the ratio of near field tip-enhanced Raman intensity to the far-field Raman signal intensity, and is given by Eq. (1) (Schmid et al., 2007; Tarun et al., 2009):

$$C = \frac{I_{near}}{I_{far}} = \frac{I_{total} - I_{far}}{I_{far}} = \frac{I_{total}}{I_{far}} - 1 \tag{1}$$

in which, the I_{near} indicates the intensity of the near-field Raman signal from the region just below the tip apex, I_{far} denotes the far-field Raman signal intensity as the tip is withdrawn, and I_{total} is the TERS experiment detected Raman intensity, which is the mixture of the near-field and far-field Raman signal intensity. The contrast can be regarded as the SNR of the TERS detection. It reflects the excitation/collection efficiency and the detection ability of the system.

In certain studies, the ability of the tip induced Raman signal amplification tends to be more concerned, and it is known as the enhancement factor. Taking into account of the difference between the sizes of the regions that give rise to the near-field and far-field Raman signal, the enhancement factor can be expressed as (Schmid et al., 2007):

$$EF = contrast \times \frac{V_{focus}}{V_{tip}} = contrast \times \frac{A_{focus} \cdot h_{focus}}{A_{tip} \cdot h_{tip}} = contrast \times \frac{d^2{}_{focus}}{d^2{}_{tip}} \times \frac{h_{focus}}{h_{tip}} \tag{2}$$

where V_{tip}, A_{tip}, h_{tip}, d_{tip} and V_{focus}, A_{focus}, h_{focus}, d_{focus} represents the near-field on the tip apex and far-field illuminated at the focus sample volume, the cross-sectional area of the illumination, radius and penetration depth of the illumination respectively. These parameters mentioned above are difficult to be accurately measured in experiment and are estimated based on the experimental conditions generally.

EF can be regarded as the normalized contrast according to the near-field/far-field signal excitation regions. It is more suitable for comparing with the electromagnetic simulation to analytically investigate the performance of the tip and the enhanced mechanisms.

Since only the Raman signal from the region just below the tip apex can be enhanced, the effect in the near-field region is estimated in accord with the size of the tip apex whose diameter is only tens of nanometers generally. But the diameter of the laser focusing spot is usually in submicron region. As a result of the great difference between the size of the near-field and the far field illumination, the experimentally obtained EF is usually about 10^3~10^6. There are still some gaps in the comparison of the electromagnetic simulation expected and experiments.

Presently, the reported EF obtained in experiment can be as high as 10^9, and some research has achieved the single-molecule lever detection (Hayazawaet al., 2006; W. H. Zhang et al., 2007; Steidtner & Pettinger, 2008). Different forms of the formula should be applied to calculate the EF of samples with different sizes and transparency. The schematic of samples with different thickness and the corresponding EF estimation formula is shown in Fig.7. For thin samples (Fig. 7(a)), since the penetration depth of the near-field and the far-field illumination are the same, the excitation region is determined just by the far-field focal spot radius or the tip radius respectively. For thicker Raman active material (Fig. 7 (b)), the impact of the different penetration depth has to be taken into consideration. Due to the far-field illuminated sample volume is much larger than the tip excitation region, when the EF

of the tip-enhancement is small the near-field signals may be submerged in the far-field background noise, and results in low contrast. The phenomenon has been confirmed in experiments (Mehtani et al., 2005). Strictly speaking, for the nano-dots and nano-wires, the TERS enhancement factors should also be estimated by using different formulas. Due to the differences between samples, the calculation of the EF is influenced by subjective factors. And the contrast, which is calculated just based on the experimentally measured values is of more practical significance. Nevertheless, the EF is still very necessary for the research on the electromagnetic enhancement mechanism of TERS. In 2005, Pettinger et al (Pettinger et al., 2005) ingeniously designed an experiment to avoid the subjective factors mentioned above. By comparing the photobleaching time of the single-layer Malachite green dye with and without tip enhancement, the more accurate TERS enhancement factor is obtained as about $6x10^6$.

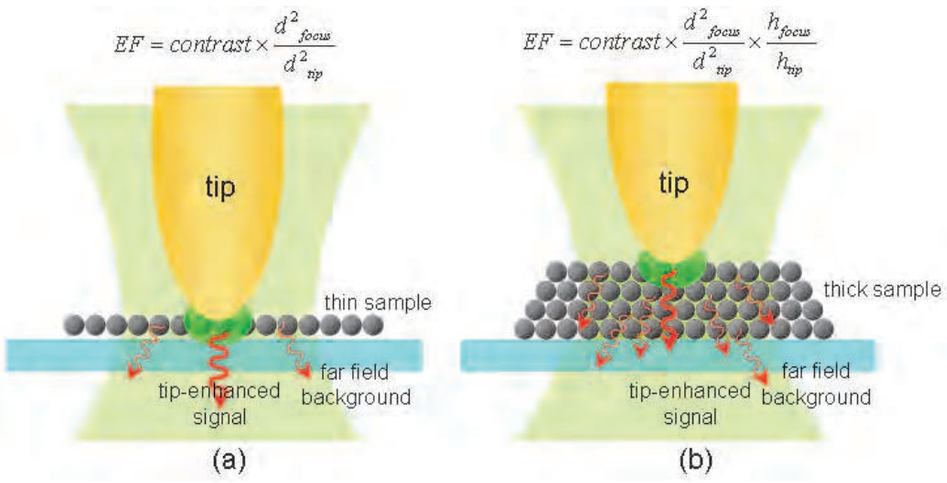

Fig. 7. Comparison of enhancement factor calculation (a) thin sample and (b) thick sample.

The lateral spatial resolution of TERS spectral imaging is mainly determined by the radius of the tip apex. Since the localized electromagnetic field enhancement is highly confined to the tip apex, the lateral resolution, spectral resolution may even be better than the resolution of topography. Nowadays, the highest lateral resolution of TERS image reported is less than 15 nm (Anderson et al., 2005). For improving the lateral resolution the topography and spectral imaging, tips with smaller radius should be used. Moreover, these tips are capable of contributing more to the tip-enhancement and field enhancement (Downes et al., 2008).

3. Preparation of CNTs specimen

Specimen preparation is an important link of applying the TERS method to the detection of practical specimens. It will finally determine whether the optimal measurement results can be obtained as well.

3.1 Requirement of specimen preparation

The in-situ non-destructive spectral detection with high resolution and high sensitivity may be accomplished with TERS system. Since the Raman spectrum directly reflects the chemical information of samples, the specimen in TERS detection is dispensed with extra label. In

general, the specimen preparation, especially for the preparation of CNTs samples, needs to satisfy following requirements:

a. The smooth substrate surface. The fluctuations of the substrate surface should be less than the sample-size scale.
b. Firmly attaching and immobilizing the specimen to the substrate surface.
c. Transparency. When using transmission-mode TERS system to detect the sample, the specimen on the substrate should be transmission. The specimen can be highly dispersed or diluted to obtain good transparency. However, in reflection-mode TERS system the detected specimen is regardless to its transparency.
d. conductivity (STM-TERS)

According to specific samples and measuring conditions, there might be certain additional requirements for the specimen preparation.

3.2 Common preparation methods for CNTs specimen

In our transmission-mode TERS system, the laser illuminates the sample from the bottom and goes through the specimen to focus on the tip apex and locally excited Raman scattering at the specimen surface. Additionally, the enhanced Raman signal also has to transmit through the specimen to be collected. Therefore, the detected specimen is optimal to be of good transparency. The CNTs specimen can be highly dispersed into a thin film. Meanwhile, the sample is required not to chemically react with the substrate or the tip and maintaining stabile properties in the whole measuring process. The specimen should also be firmly attached on the substrate surface to avoid relative movement during the scanning. In order to obtain high-resolution images, highly dispersed samples are generally used. Therefore, the transmission-mode TERS system is more suitable for detecting sparse thin films of CNTs samples with good transparency. For example, the specimen preparation methods used in our transmission-mode TERS detection are presented here.

3.2.1 Preparation method for single wall carbon nanotube sample (SWNTs)

The SWNTs specimens used in our experiments are bundles of SWNTs. The SWNTs were synthesized by arc-discharge method. After purification, the high purity (> 95%) SWNTs powder can be obtained. Then 0.01mg powder was dissolved in 10mL ethanol. The solution was evenly dispersed by ultrasonic dispersing method. One droplet of the solution was taken and dripped on a 120μm thickness cover slip. After air-curing, the transparent CNTs specimen has been prepared as well as for detection (Guan, 2006; Li et al., 2004).

3.2.2 Preparation method for double wall carbon nanotube sample (DWNTs)

The transparent thin DWNTs membrane was prepared following the series of processing (Wei et al., 2006): firstly, the synthesized DWNTs were soaked in the H_2O_2 solution with 30% Concentration for 72 hours. Then, HCl solution (37%) was added to remove the amorphous carbon, catalyst particles and other impurities. The up to 90% (by mass fraction) purity DWNTs were obtained. By dripping several drops of ethanol or acetone, the purified macro-membrane of DWNTs were rapidly spreading to ultra-thin film and floating on the surface of the solution. The film of DWNTs can be easily collected with a cover slip. The flat and transparent thin film of DWNTs was obtained, and after air-curing the highly dispersed DWNTs were immobilized on the substrate surface.

4. Detection of CNTs

The TERS technology has been widely developed and applied in the fields of physics, chemistry, material science, and biology in nanometer scale. Especially, the detection of CNTs will be presented and discussed as an emphasis of this section.

4.1 Applications of TERS

The significant advantage of TERS is that it can provide corresponding topography and Raman mapping of the nano-material specimen with high spatial resolution and detection sensitivity. Since 2000, TERS has been experimentally proved practicable (Stöckle et al., 2000; Hayazawa et al., 2000; Anderson, 2000; Pettingeret al., 2000) and shows the potential of nanometric spectral detection. Then, the research on TERS's applications has been being advanced continually.

Up to now, it has been applied to dye molecule detection (Steidtner & Pettinger, 2008; W. H. Zhang et al., 2007), semi-conductor material determination(Sun et al., 2003; Lee et al., 2007; Saito et al., 2008; Sun & Shen, 2001) , biological specimen identification(Anderson et al., 2003; Watanabe et al., 2004; Bailo & Deckert, 2008), and nanao-material characterization (Hayazawa et al., 2000; Hartschuh et al., 2003; J. J. Wang et al., 2005; Qian et al., 2006).

It is distinct from the single molecule level or single-molecule state distributed specimen detection, TERS approach aims on the real single molecule, individual molecule Raman spectral detection. In 2008, Pettinger et al. directly measured the spatial location and the corresponding Raman spectra of the single BCB molecule absorbed on Au (111) surface using STM-TERS system in ultra-high vacuum (Steidtner & Pettinger, 2008). The experiment shows that under resonance Raman excitation, the enhancement factor is to 10^6. It is enough to satisfy the requirement of the single molecule detection sensitivity of the dye molecules in the TERS characterization.

The in situ spectrum detection of biological samples is another research hotspot in TERS applications in recent years. Since the Raman spectra directly reflect the molecular structure information of the sample, the specimen in TERS detection is dispensed with extra label. Meanwhile, TERS is capable of obtaining high resolution in situ non-destructive detection with high sensitivity. In 2003, Anderson et al. (Anderson et al., 2003) applied TERS technique to the detection of drosophila compound eyes, and measured the fine structures of the eye surface and the near-field Raman spectra at different positions. In 2006, Hayazawa et al. (Hayazawa et al., 2006) measured the near-field Raman spectroscopy of the adenine nano-crystal sample. Compared with the standard far-field spectrum, slight frequency shift of the TERS spectra is reviewed. In 2008, Bailo et al. (Bailo & Deckert, 2008) detected the topography of single-stranded cytosine RNA and its tip-enhanced Raman spectra at several different positions. The single-base detection sensitivity of the TERS system is indirectly proved. The author further noted that although the TERS system is not yet sufficient to the spectral imaging with the single-base spatial resolution, TERS technology is still expected to directly sequence the DNA or RNA samples by using certain detection and data processing method. TERS research on live Biological macromolecules and virus has been commenced. Recently, Deckert et al. (Cialla et al., 2009) measured the TERS signals of the single tobacco mosaic virus at different positions, and the characteristic Raman shifts were identified. Budich et al. (Budich et al., 2008) also reported the TERS characterization of the Staphylococcus epidermidis cell wall in liquid environment. These applications all indicate the great potentials of the TERS technique in biological and life science research.

The demand of nano-material characterization is a major motivation to promote the development of TERS. CNT is a kind of the typical 1-D nano-materials. Much attention has been paid to the research and detection of CNT, Due to its outstanding physical, mechanical, thermal and electrical properties along with application potentials. In 2003, Hayazawa et al. (Hayazawa et al., 2003) applied TERS method to detect the SWNTs specimen and obtained the diameter and chirality of the CTNs by analizing the TERS reaults. Harschuh et al. (Hartschuh et al., 2003) also utilized TERS to characterize SWNTs and simultaneously acquired the topography and the TERS mapping. Comparing the features in the two images, the spatial distribution of the CNTs can be accurately recognized. In this detection, the spatial resolution of TERS mapping reached up to 23 nm, even better than that of topography, which is 29 nm. With the development of the tip preparation and the TERS realization, better than 15 nm TERS resolution can be achieved nowadays (Hartschuh et al., 2005; Anderson et al., 2005; Huihong et al., 2008: 2243-6). In 2005, Hartschuh et al. measured the TERS and tip-enhanced photoluminescence (PL) mapping of SWNTs with better than 15 nm resolution (Hartschuh et al., 2005). The structural defects and optical properties of CNTs may be further revealed with the combination of TERS detection and tip-enhanced photoluminescence (PL). In 2006, Kawata et al. imaged SWNTs bundle within 700 nm×700 nm region. It validated that the radial breathing mode (RBM) feature inducing the Raman shift corresponding to the vibrational mode of the graphitic layer in the radial direction is sensitively and directly depended on the diameters of the tube. By imaging a serial of TERS mappings according to different RBM Raman shifts, the distribution of SWNTs with different diameters can be obtained separately. Lately, Kawata's group reported another way to further improving the resolution of TERS. In this method, the CNTs below the tip are locally pressed by the tip apex, and the slight Raman frequency shift induced by the pressure can be accurately detected. The technology is employed in nanometer metrology and spatial resolution is to 4 nm (Yano et al., 2009).

Carbon nanotubes are categorized as single-walled nanotubes (SWNTs), double-walled nanotubes (DWNTs) and multi-walled nanotubes (MWNTs). According to the difference in sizes, structures and features of them, SWNTs and MWNTs will be measured. Also experimental examples will be provided and discussed respectively in the following passages.

4.2 Detection of SWNTs

Generally speaking, the Raman peaks of SWNTs spectra represent the major vibration modes in CNTs, the radial breathing mode (RBM), graphite-like mode (G-mode corresponding to G-band), and defect-related mode (D-mode, D-band)(Dresselhaus et al., 2005; Rao et al., 1997).

The Raman shifts related to RBM is at the low frequency region of the spectrum. They are associated with the radial direction vibration modes of the nanotubes and directly reflect the diameters of the SWNTs. The G-mode vibrations of SWNTs are induced by the planar vibrations of the carbon atoms. The G-mode vibrations bring in Raman shifts in G-band, which is generally around 1600 cm^{-1}. Also most graphite-like materials all generate the G-band in Raman spectra. The D-mode of CNTs is related to the out-of-order defects of the CNTs or the amorphous carbon in the sample. The D-mode vibrations of SWNTs result in the Raman shifts around 1300 cm^{-1}. The ratio of G-band to D-band is an important term for the evaluation of the purity of the SWNTs specimen (Eklund et al., 1995).

4.2.1 Conventional Raman spectrum measurement of SWNTs

For comparison and calibration, the conventional far-field Raman signal of the SWNTs specimen was measured before the TERS detection. The photon-counter integrated time is set 100ms in the Raman spectroscope, Renishaw RM2000. The result is shown in Fig. 8(a). From the far-field Raman spectrum, several Raman shift feature peaks of the SWNTs specimen can be distinguished. One is the G-band corresponding to the planer vibration. It breaks up to several characteristic peaks as the fold in Brillouin Zone and mainly represents as G^+ band in the high frequency region (1592 cm^{-1}) and G- band in the low frequency region (1569cm^{-1}). Second is the D-band at 1347 cm^{-1}, which is resulted from amorphous carbon or out-of-order defects in SWNTs sample. The purity of SWNTs sample can be evaluated based on the ratio of G band and D band (Dresselhaus et al., 2005). As the experimental result indicated, the ratio of G and D band of the specimen is 26.

Another characteristic Raman shift corresponding to RBM was detected in low frequency region and accumulated 3 times with the integrated time, 10 seconds. Considering that the sample is bundle of SWNTs and the tube-tube interaction in the bundle, the relationship between the diameter d_t (nm) of the nanotube and the RBM band ω_{RBM} (cm^{-1}) can be expressed as following (Rao et al.,2001),

$$\omega_{RBM} = 224/d_t + 10 \tag{3}$$

This is a modified formula for a bundle of SWNTs slightly different from isolated SWNTs. As the detected RBM frequency is 170cm^{-1} (Fig. 8 (b)), the diameter of the SWNTs is estimated to be 1.4 nm.

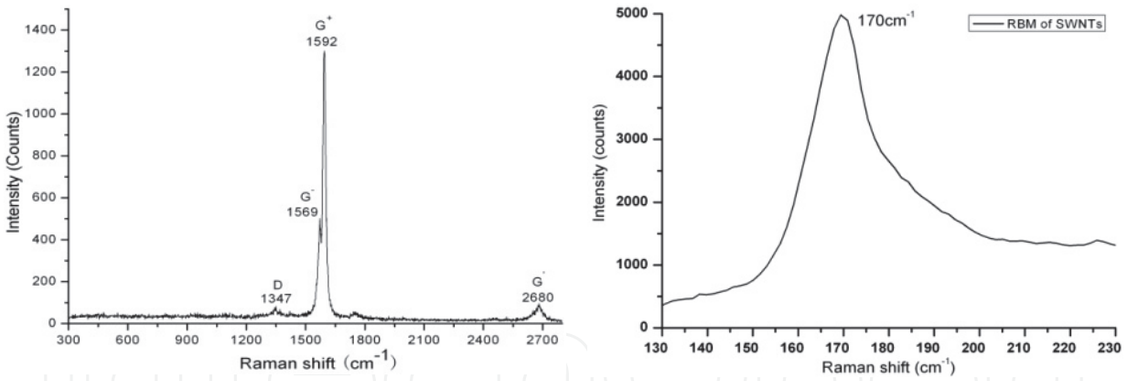

Fig. 8. (a) Raman spectrum of SWNTs (b) RBM of SWNTs

4.2.2 Topographic and TERS measurement of SWNTs bundle

The SWNTs specimen is detected with a transmission-mode TERS system based on an AFM. Firstly, the topography of the SWNTs specimen is obtained by AFM (Fig.9). It can be indicated that in the sample most SWNTs exist in the form of bundles due to the action of Van der Waals force. On the SWNTs bundle one position marked with cross is selected as the interest point of TERS detection. Then, the position of the specimen is relatively moved to the near-field region and just below the metallized tip apex. The TERS spectrum of the SWNTs specimen is shown in Fig.10 (a). Then, the far-field Raman spectrum at the same position is detected (Fig.10 (b)), as the tip is withdrawn from the near-field region of the specimen (Wu et al, 2009).

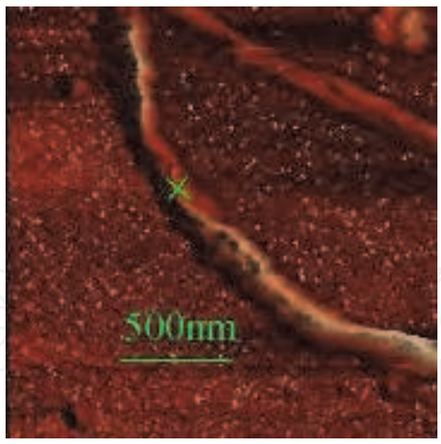

Fig. 9. Topographic image of a Single SWNT bundle with diameter 100nm, by TERS.

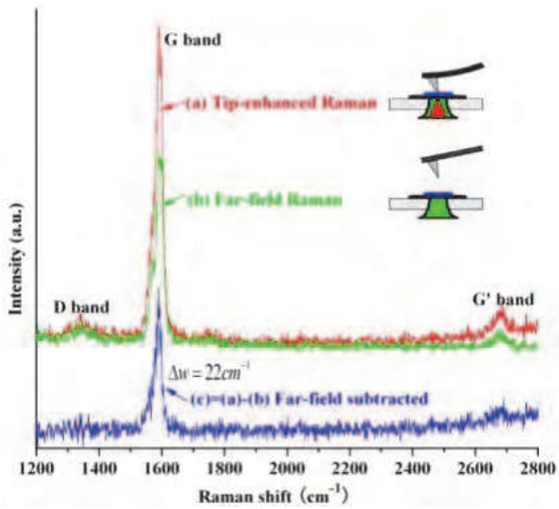

Fig. 10. TERS and far-field Raman spectra of a single SWNT bundle.

Comparing the TERS spectrum with the far-field Raman spectrum, it can be noticed that the frequency of G-band Raman peak is not obviously shifted and the shape is not evidently changed. In addition, the characteristic G-band is considerably enhanced as a result of the tip-enhanced electromagnetic field, while the background noise is not obviously increased. This can be explained as that the noise is mainly comes from the far-field stray light in the illuminated area and not Raman scattering localized and enhanced by the tip. While Raman signal from the localized zone is greatly enhanced by the tip-enhanced electromagnetic field highly confined to the tip's apex. It results in the higher SNR detection results. The pure near-field Raman signal of SWNTs can be obtained as shown in Fig.10(c), by subtracting the far-field signal from the TERS spectrum. The enhancement factor is calculated to be 230 according to the formula given in Fig. 7 (a) for thin film specimens. The tip enhancement factor will be much larger than that value, because the practical diameter of far-field laser spot is always larger than the size of the diffraction-limit used in the estimation. It indicates adequately that TERS technology is of novel and excellent performances in detection of weak Raman signal in nanometer localized region.

4.3 Detection of MWNTs

Multi-walled nanotubes (MWNTs) are formed with multiple coaxial rolled layers of graphite. Due to the structures and compositions, they have similar Raman shifts with SWNTs, but still with several distinct features. Additionally, being the simplest manifestation of MWNTs, the double-walled carbon nanotubes (DWNTs) are considered to be an ideal model for researching the interaction between graphite layers, as well as the connections between the SWNTs and MWNTs.

4.3.1 Detection of DWNTs

A DWNT has the structure of two coaxial hollow cylinders formed by two layers of rolled-up graphite. The typical interlayer space between the inner and the outer walls, ranges from 0.33 nm to 0.42 nm. DWNTs maintain several outstanding properties of SWNTs, yet have some distinct ones, such as higher stability and particular electronic and optical properties (Gennaro et al., 2009). In Raman spectra of DWNTs, the graphite-like band (G-band) region arose by the graphitic layers is regarded as one of the feature Raman shifts of CNTs. And the RBM frequency corresponding to the radial direction vibration of the nanotubes is sensitively and directly depending on the diameters of the inner and the outer walls.

In this practical example, DWNTs specimen was investigated using our home-made transmission-mode TERS system (Wu et al., 2010). The Raman enhancement factor was calculated. The tip-enhanced Raman spectra especially in the G-band and the RBM regions are obtained. A tip-pressure induced RBM band shift of the DWNT is observed, and the experimental results are discussed.

In this research, a backward-scattering TERS system with a golden AFM tip is used. The radius of the tip apex is about 30 nm. The DWNTs specimen is prepared using the method mentioned in section 3.2.2. And the DWNTs used here were synthesized by chemical vapor deposition (CVD) process. In TERS detection, the excitation laser (532 nm) after expanding and collimating is focused on the tip by a high-NA objective (NA = 0.95). Also the tip-enhanced Raman scattering from a confined region of the specimen is efficiently excited. Then the Raman scattering is collected by the same objective lens and channeled into the Raman spectroscope to be analyzed.

In advance, the topography of the DWNTs specimen was detected (Fig. 11(a)). The height cross section along the dashed line is shown in Fig. 11(b). It shows that the heights of the 3 figures are all about 10 nm. Judging from the height, the two arc-like bundles each contains

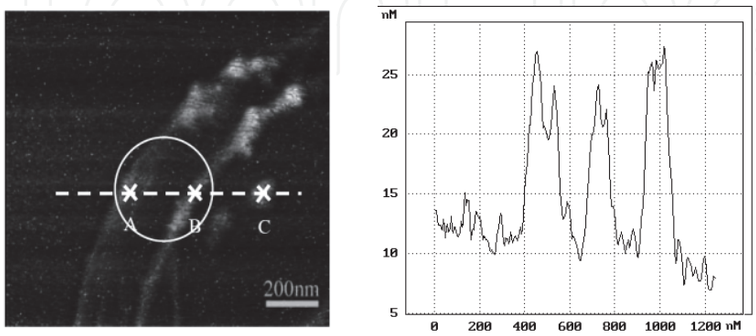

(a) (b)

Fig. 11. (a) Topographic image of the DWNTs specimen (scanning area: 1.2 μm × 1.2 μm). (b) Height cross section along the dashed line in (a).

estimated about 10 to 15 DWNTs. After acquiring the topography of the specimen, the region-of-interest could be narrowed down and defined to the three figures. Then, the single-point TERS detection was carried out at each interested position. The detected TERS spectrum of position A of the specimen is shown in Fig. 12. For comparison, the far-field Raman spectrum was detected as the tip was withdrawn from the near-field region. The separation between the tip and the sample surface was about 1.5 μm then.

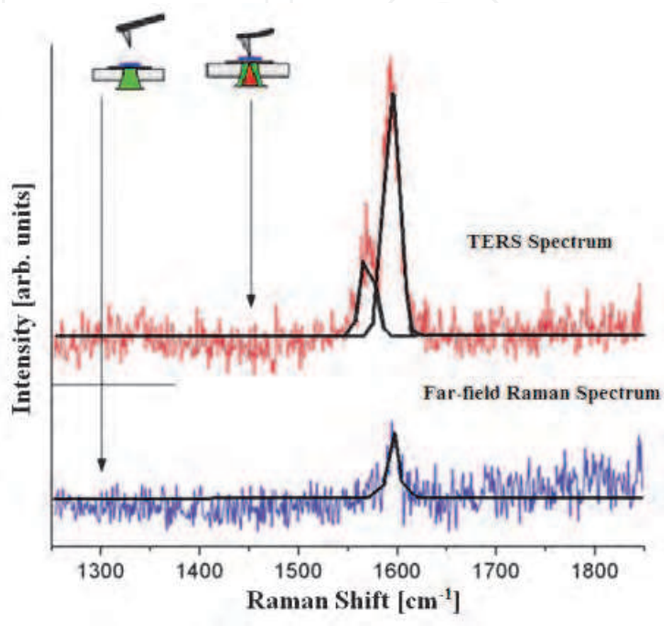

Fig. 12. Far-field Raman spectrum and TERS spectrum of DWNTs at position A in Fig. 11(a).

Compared with the far-field spectrum, the TERS spectrum indicates that a strong enhancement at the G-band is obtained. With Lorentz fitting, it can be observed that the G band in the TERS spectrum splits mainly into two peaks: 1590 cm^{-1} (G^{+}) and 1564 cm^{-1} (G^{-}). However, in the far-field Raman spectrum the G^{-} band may be too weak to be distinguished from the noise. According to the Eq. (2) given in section 2.4, the EF is calculated to be 3.6×10^{2}.

With the tip fixed at the laser focus, the specimen is moved along the dashed line shown in Fig. 11(a). The TERS spectra of positions A, B, and C are detected in succession (shown in Fig. 13). TERS spectra of positions A and B both show similar Raman peaks in the G-band and almost no signals in the D-band. However, at position C the Raman peak in the D-band is strong and the G band signal is weak. By comparative analysis of the topography and the TERS spectra it can be ratiocinated that the two arc-like lines are bundles of DWNTs, while the granule at position C is amorphous carbon respectively. The Raman signal from C includes the D-band from amorphous carbon and the weak G-band signal might from DWNTs in the vicinity of C point illuminated area in the far-field.

For further characterization of DWNT specimen, the Raman spectra in the RBM region were detected and analyzed to estimate the diameters of the DWNTs' inner and the outer walls, respectively. The Raman shift in RBM region can be directly determined from the diameter of the nanotube. Thus, it's quite useful in estimating the sizes of the inner and the outer walls of DWNTs and the corresponding deformation of DWNTs under radial pressure.

Since the interaction between the inner and the outer walls and the force exerted between two DWNTs will both induce upshift to the frequencies of the Raman shifts in RBM band (Bandow et al., 2002), the formula $\omega_{RBM} = 224/ d_t$ with about 10% higher RBM frequency modification is adopted here to calculate the corresponding diameter of the nanotubes, as Eq. (3) above similar to SWNTs.

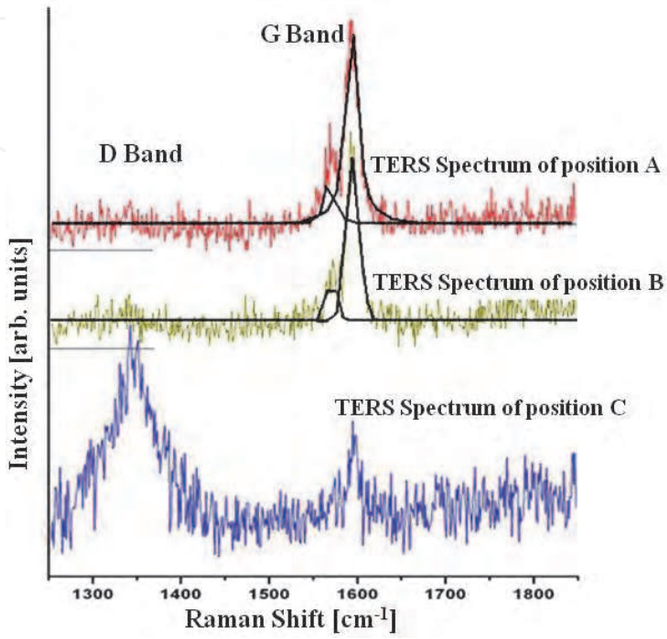

Fig. 13. TERS spectra at the 3 positions (A, B, and C) marked correspondingly in Fig. 11(a)

The experimental obtained RBM band consists of two groups of Raman shift peaks, the range from 140 cm^{-1} to 160 cm^{-1} and 250 cm^{-1} to 270 cm^{-1}, which can be observed in Fig.15 (far-field) and Fig.16 (tip-enhanced). Since the RBM frequency depends inversely on the nanotube diameter, the two groups of peaks correspond to the outer and the inner walls of DWNTs respectively. The calculated diameters of the nanotubes are shown in Table 2. The outer walls' diameters vary between 1.51 nm and 1.69 nm while the inner walls' diameters vary between 0.89 nm to 0.93 nm.

In this experiment, the topography of another selected area of the DWNTs sample was detected by using AFM (shown in Fig. 14) before the Raman spectral investigation. Two arc-like bundles of DWNTs, whose heights were 3 nm and 6 nm respectively, were observed in the detected area. With the tip withdrawn from the near-field of the sample, the far-field Raman spectrum of the DWNTs was obtained (as shown in Fig. 15). Then, for further detection of the tip-enhanced RBM of the DWNTs, the AFM golden tip was approached to the near-field of the sample, and the scanning stage was precisely moved to align the interested DWNT bundle with the tip's apex. After eliminating the far-field background, the tip-enhanced RBM of position A and B are shown in Fig. 16(a) and (b) respectively.

Comparing the tip-enhanced RBM with the far-field one, one can draw two conclusions. First, the excitation area is highly confined. Seven peaks in the RBM region are detected from the far-field Raman spectrum while 5 and 7 peaks are detected at the position A and B in TERS, respectively.

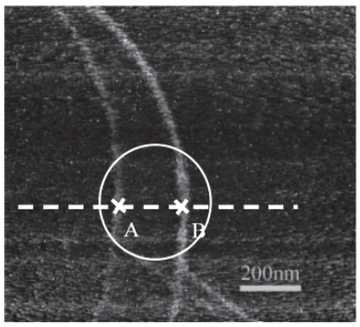

Fig. 14. Topographic image of DWNTs.

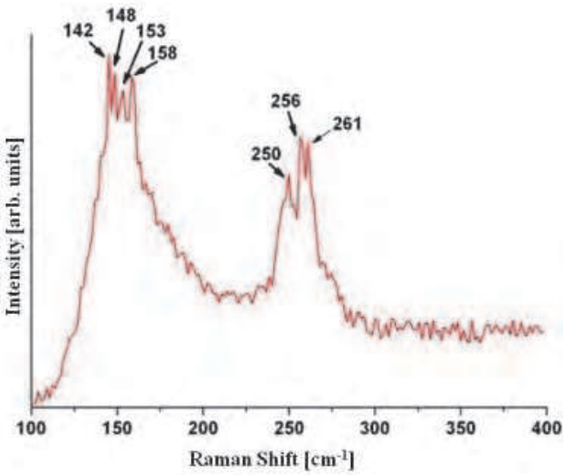

Fig. 15. Far-field Raman spectrum of a DWNT in the RBM region.

outer wall		inner wall		interlayer space (nm)
Raman shift (cm^{-1})	Diameter (nm)	Raman shift (cm^{-1})	Diameter (nm)	
142	1.69	250	0.93	0.38
		256	0.91	0.39
		261	0.89	0.40
148	1.62	250	0.93	0.345
		256	0.91	0.355
		261	0.89	0.365
153	1.57	261	0.89	0.34
158	1.51	-	-	-

Table 2. Correspondence of the far-field RBM frequencies and the diameters of the DWNTs.

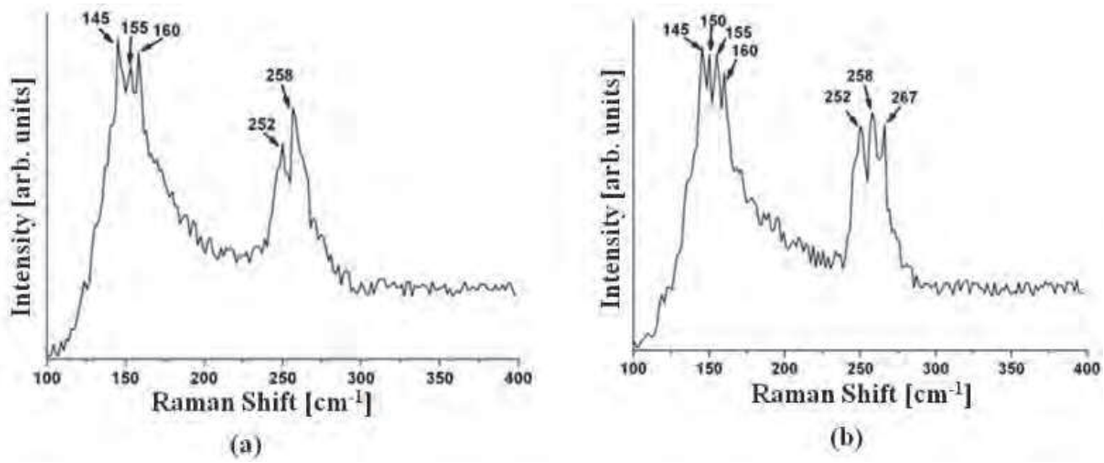

Fig. 16. The tip-enhanced RBM from (a) A point and (b) B respectively after subtracting the far-field background.

Far-field (cm^{-1})	Position A (cm^{-1})	Position B (cm^{-1})	Peak shift (cm^{-1})
142	145	145	3
148	-	150	2
151	155	155	2
158	160	160	2
250	252	252	2
256	258	258	2
261	-	267	6

Table 3. Contrast of the far-field and the tip-enhanced Raman shift of RBM.

As the Raman shifts in RBM bands directly reflect the diameters of the nanotubes, this indicates that the left bundle includes more assembled forms of inner and outer walls than the right bundle at A. This also demonstrates that, in the TERS method, the Raman spectrum can be efficiently enhanced in a highly-confined volume and that the RBM of each bundle can be detected separately. Second, the slight shift in RBM is observed and is related to the deformation of DWNTs caused by the tip pressure. The tip-enhanced RBM bands at A and B reflect 2 to 3 cm^{-1} upshifts compared with the initial ones shown in the far-field Raman spectrum. Considering the systematic residuals and random error in experiments, the measurement was taken several times with the scanning stage aligning the position of

interest in the mode, and the tip scans from left to right and then from right to left. The results obtained for the tip-enhanced RBM bands are all in good agreement, and it indicates that the Raman shift phenomenon is repeatedly measured. The peak shift between the tip-enhanced RBM bands and the far-field RBM bands is related to the deformation of DWNTs and may be attributed to a combination of the tip mechanical pressure and the interaction between the two walls of the DWNTs.

For further experimental investigation on the dependences of the band shift and the intensity of TERS on the pressure should be carried out. That would provide further qualitative and quantitative analyses of the external pressure effects and the internal force interactions of the DWNTs. Also, the stress distribution in the DWNTs should be obtained by TERS mapping measurement. It can be assumed that the interacting force between the two walls of the DWNT under tip pressure can be achieved by measuring the tip-enhanced RBM bands shift.

4.3.2 Detection of MWNTs

In this detection, a single MWNT was investigated with our home-made side-illumination reflection-mode TERS system (R. Wang et al., 2010a). An Ag coated optical fiber probe fabricated in the chemical method was used. The experimental results indicate that the measuring system has a spatial resolution better than 70 nm, and the enhancement factor is about 5×10^3.

The laser beam form a Nd:YAG laser, wavelength 532 nm is focused on the probe tip by a long work distance objective (50×, NA=0.42, WD=20.5mm, Mitutoyo) at the incident angle of 65° relative to the axis of the probe. The polarization of the incident light is along the axis of the probe to get stronger enhanced field on the tip apex. The separation between the tip and the sample is kept constant and less than 5 nm by the shear-force feedback control. The Raman scattering is collected by the same objective. Then it is steered into the Raman spectroscope, Renishaw RM2000, and detected by a cooled CCD detector. The measured wavenumber range from 4000 to 100 cm^{-1} is determined by the band width of the edge filter.

In this experiment, the samples under test were water dispersible MWNTs (Shenzhen Nanotech Port Co. Ltd) with the tube diameters of 20 ~ 40 nm. After further diluted with deionized water and dispersed with ultrasonic, the sample solution (~ 0.2 wt. %) was dropped on the surface of the silicon wafer and dried.

A topographic image of a single MWNT was obtained, as shown in Fig. 17(a). A cross section along the dash-dot line in (a) is shown in Fig. 17(b). It is clearly indicated that the height of the MWNTs is about 40 nm. The diameter of the single MWNT is markedly broadened to 100 nm due to the geometry of the tip. Three points A1, A2, and A3 with the intervals of ~70 nm are chosen on the three crosses and the TERS information on the three points is detected respectively.

The TERS spectra with tip and far-field Raman spectrum without tip are displayed in Fig. 17(c). The two peaks (about 1300 cm^{-1} and 1600cm^{-1}) are corresponding to the defect-related mode (D mode) and graphite-like mode (G mode) respectively. Among the TERS spectra at A1, A2 and A3 the distinct differences can be observed. Point A1 and A3 locate brims of the tube respectively and it leads Raman peaks unobvious. Point A2 just locates on the carbon tube and there is a stronger Raman peaks in the TERS spectrum. It demonstrates experimentally that the spatial resolution is better than 70 nm with the TERS system.

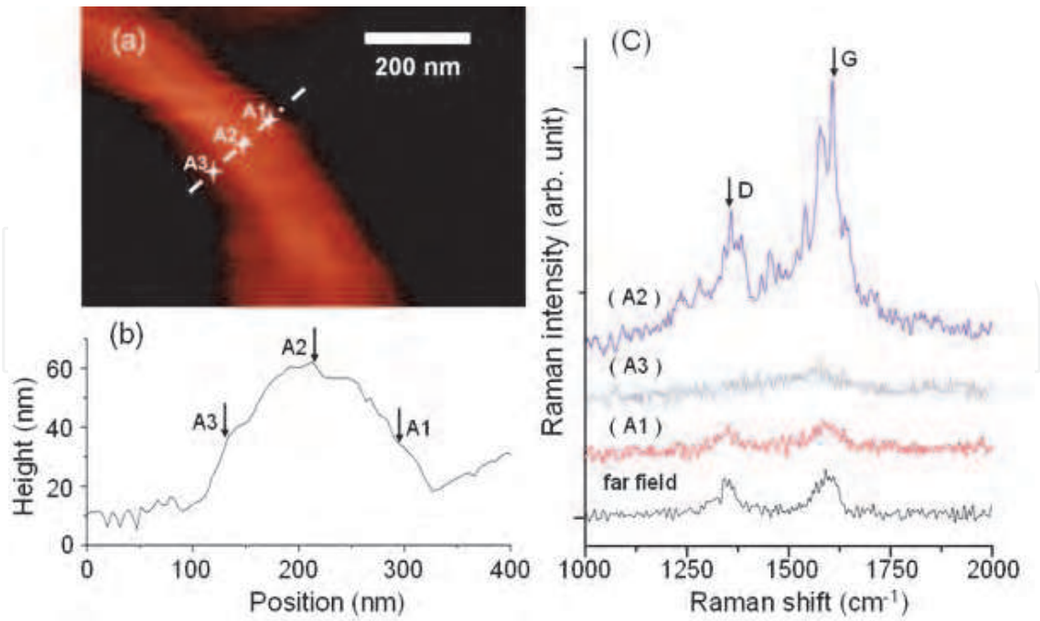

Fig. 17. TERS measurement results of a single MWNT. (a) topographic image of a single MWNT; (b) corresponding height-cross-sections along three measuring points marked in (a); (c) tip-enhanced Raman spectra of the MWNT at different points and the far field Raman spectrum of the whole area.

The comparison between the TERS Raman intensity at point A2 and the far-field Raman intensity shows that the former has 5-6 times intensity than the latter. Considering the radius of the tip and the size of laser focusing spot, the tip-enhancement factor is about 5×10^3. Although both tip-enhanced Raman spectra and far-field Raman spectra show the inherent Raman peaks of MWNTs, spectrum at A2 seem to have more fine features. It is probably from the structure defect or the interaction between the tip and the MWNTs.

4.4 TERS mapping

One of the significant superiority of TERS is that it provides the topography and the Raman spectral mapping simultaneously and the two images can be correspondingly recognized. To obtain the spectral signal from the interested localized region in nanometer scale on the sample and further investigate the chemical information from the nano-structure in the area, the TERS mapping is useful and necessary. In TERS mapping, the metallized tip scans point by point over the interested area of the specimen and the full spectra in each detected point are acquired. Then the specific Raman peaks or bands, which directly reflect the feature of the interested material structure are picked out, and subsequently set as reference to identify the composites and the molecule structure in the Raman spectral mapping. The spectrum of each position is analyzed and intensity of the Raman peaks is marked in the corresponding position of the mapping. T. Yano et al utilized TERS to measure the distribution of SWNTs with a spatial resolution far beyond the diffraction limit. The RBM of SWNTs in the near-field Raman spectra is corresponding to the diameters of various SWNTs in the immediate vicinity of the tip. The near-field Raman imaging of the RBM provided a super-resolved color mapping corresponding to the diameter distribution of SWNTs within a bundle (Yano et al., 2006).

In experiment, the detection of Raman spectrum needs a few seconds to a few minutes accumulation time to obtain the spectrum signal with the higher ratio of signal and noise. With the increase of the TERS mapping area, the number of points to be detected grows up rapidly. Thus, intending to obtain a high resolution TERS mapping in a comparatively large area, may require up to an hour or even more. Therefore, the long time stability of the TERS system is quite critical (as discussed in section 2.3.3).

The TERS mapping of a Cr grating on a Si wafer and its corresponding topography is presented as shown in Fig.18. The measuring area is 300 nm × 1200 nm and the sampling point of TERS mapping is 4 points × 12 points with the interval about 100nm. The accumulation time at each point is ten seconds, and the total detecting time of TERS is about 25 minutes. The picked reference Raman peak is 520 cm^{-1}, which corresponds with Si. Thus, the TERS mapping shows the distribution of Si in the detected area. As shown in Fig.18, the spatial relationship between the topography and the Raman mapping demonstrates that the TERS mapping can provide the correspondent recognition of physical and chemical information (R. Wang, 2010b).

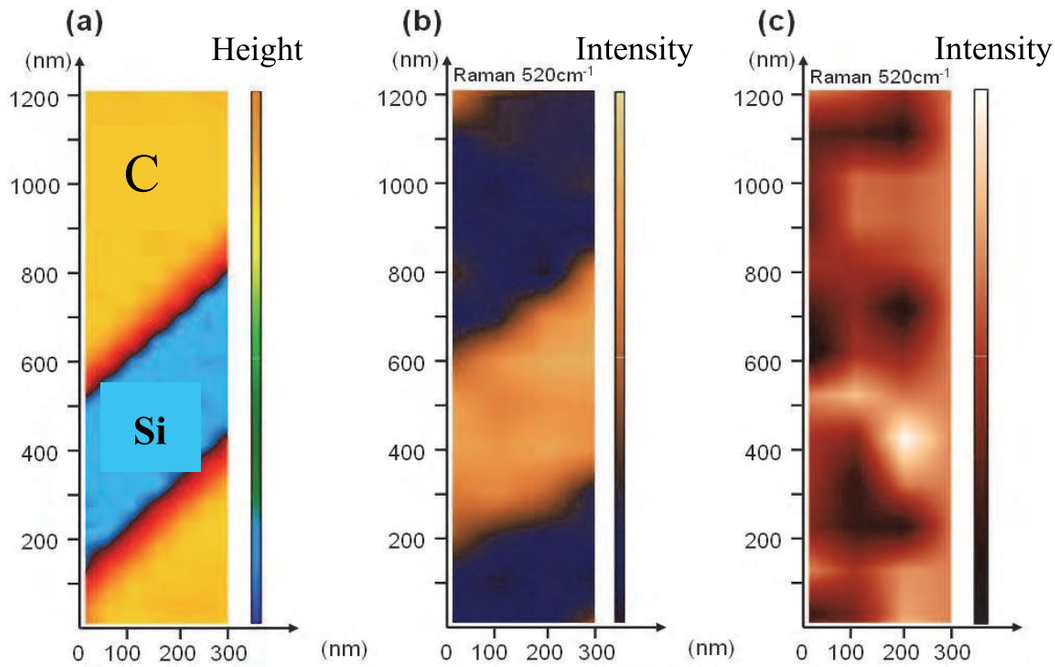

Fig. 18. (a) The topography (b) the TERS mapping and (c) far-field Raman mapping of the Si/Cr grating.

5. Conclusions

As a tip-enhanced spectroscopy, TERS system combines SPM (STM, AFM, SFM, SNOM) scanning head, Raman spectroscope, optical microscope, control units and data acquirement into a complicated topography and spectral measuring system. TERS is employed not only to detect Raman spectrum from nanometer localized volume, but also topographic data corresponding to the former in nanometer accuracy simultaneously. TERS mapping and spectral imaging become the important analysis method in nano-material science research.

TERS has become the promising tool in the nanometric Raman spectrum recognition and identification.

There is no doubt that TERS is a strong tool in the measurement and characterization of CNTs. Some SWNT bundle samples are measured and characterized with the TERS system. The topography of SWNTs is obtained, and SWNT bundles, diameter 100nm, were synchronously measured with the TERS. The experimental results reveal that Raman spectroscopic detection beyond the optical diffraction limits has been realized. The most TERS spectrum data obtained is from three pieces of SWNTs, based on the analysis to the TERS data. Comparing TERS and far-field Raman spectrum data, the results indicate that the TERS enhancement factor is over to 230.

The DWNTs and MWNTs samples are also measured with the TERS system. The experimental results indicate that the Raman signal can be efficiently enhanced in a highly-confined volume. The RBM of each bundle may be detected separately. The Raman peaks shift between the tip-enhanced RBM bands and the far-field RBM bands is related to the deformation of DWNTs. It may be attributed to a combining process of the tip mechanical pressure and the interaction between the two walls of the DWNTs. It demonstrates experimentally that the spatial resolution is better than 70 nm and the enhancement factor is about 5×10^3.

The TERS results demonstrate experimentally that TERS technology is not only of the spatial and optical resolution beyond the diffraction limits, but also has ability to realize nanometer localization spectral detection. They have the accurate corresponding relationship and have many benefits to the spectral recognition in the nanometer localize space in the potential applications.

TERS technology has been paid much attention to and widely used in nano-science and nano-technology. Even though many achievements have been obtained with TERS, it must be noted that the TERS technology is being developed and not yet perfect. Some issues need to be further investigated in the coming research.

It has been found that, there are some slight differences between TERS spectrum and far-field micro-Raman spectrum. Up to now, the clear conclusions and common views on the mechanism have not yet been reached, although some people tried to explain it based on the gradient field effect (Ayars et al., 2000), tip polarization/depolarization effect (Gucciardi et al., 2008), optical antenna effect (Novotny, 2008), tip thermal effect (Downes et al., 2006), and pressure effect (Watanabe et al., 2004) and so on. Theoretically, it is a quite complicated issue to build an exquisite physical model and explain thoroughly the mechanism of TERS. The selection rule of TERS needs to be built under the system of nanometer metallized tip and molecule localized electromagnetic field coupling.

Some following issues on TERS might be studied in the future.

a. TERS will work under the vacuum and liquid environment (Steidtner & Pettinger, 2008). It is helpful to explore the TERS sensitivity limit and spatial resolution. It will make one to understand deeply the TERS theoretical mechanism. TERS will play an important role in life science as it gets the tip-enhanced spectrum under liquid environment.
b. TERS will be used in semiconductor inspection. It may be used in inspections for stress distribution and fission process in nanometer scale (Zhu et al., 2007a, 2007b; Georgi et al., 2007). The polarization control techniques may be used to reduce the far-field background to improve the contrast (Lee et al., 2007).

c. New and optimizing tip preparation methods will massively produce high quality tips with uniform geometry, firm metal coating, controllable optical and resonance properties, time stability, and durability to satisfy the excitation conditions (Cui et al., 2007; Yeo et al., 2006).
d. With appropriate polarization light, for example radial polarized light, as an exciting beam as mentioned above, it will further improve the spatial resolution and tip enhancement factors. It can realize the atom resolution and real single piece of SWNTs measurement.
e. Instrumentation and commercialization of TERS will be accomplished in the combination with more type probe microscopes and spectroscopes and special optical devices, such as parabolic mirror.

In summary, the TERS technology with excellent performances will become an important measurement and characterization tool in the field of nano-materials and nano-structures.

6. Acknowledgement

The authors gratefully thank all people who gave us helps in the discussions, fabrications and inspections for specimen preparations. This work was financed by the National Natural Science Foundation of China for the support under the grant 60427003, and the National Basic Research Program of China (973 Program) Grant, project research on optical detection in nanometric scale, No. 2007CB936801.

7. References

Anderson, M. S. (2000). Locally enhanced Raman spectroscopy with an atomic force microscope. *Applied Physics Letters,* Vol. 76, No. 21, pp. (3130-3132), ISSN 0003-6951

Anderson, M. S. & Gaimari, S. D. (2003). Raman-atomic force microscopy of the ommatidial surfaces of Dipteran compound eyes. *Journal of Structural Biology,* Vol. 142, No. 3, pp. (364-368), ISSN 1047-8477

Anderson, N.; Hartschuh, A.; Cronin, S. & Novotny, L. (2005). Nanoscale vibrational analysis of single-walled carbon nanotubes. *Journal of the American Chemical Society,* Vol. 127, No. 8, pp. (2533-2537), ISSN 0002-7863

Anderson, N.; Bouhelier, A. & Novotny, L. (2006). Near-field photonics: tip-enhanced microscopy and spectroscopy on the nanoscale. *Journal of Optics A: Pure and Applied Optics,* Vol. 8, No. 4, pp. (227–233), ISSN 0950-0340

Ayars, E. J.; Hallen, H. D. & Jahncke, C L. (2000). Electric field gradient effects in Raman spectroscopy. *Physical Review Letters*, Vol. 85, No. 19, pp.(4180-4183), ISSN 0031-9007

Bailo, E. & Deckert, V. (2008). Tip-enhanced Raman spectroscopy of single RNA strands: Towards a novel direct-sequencing method. *Angewandte Chemie-International Edition,* Vol. 47, No. 9, pp. (1658-1661), ISSN 1521-3773

Bandow, S.; Chen, G.; Sumanasekera, G. U.; Gupta, R.; Yudasaka, M.; Iijima, S. & Eklund, P. C. (2002). Diameter-selective resonant Raman scattering in double-wall carbon nanotubes. *Physical Review B*, Vol. 66, No. 7, pp.(75416-1-8), ISSN 1098-0121

Bohren, C. F. & Huffman, D. R. (1998). Absorption and Scattering of Light by Small Particles. Wiley, ISBN: 978-0-471-29340-8, New York.

Budich, C.; Neugebauer, U.; Popp, J. & Deckert, V. (2008). Cell wall investigations utilizing tip-enhanced Raman scattering. *Journal of Microscopy-Oxford,* Vol. 229, No. 3, pp. (533-539), ISSN 0022-2720

Chiang, I. W.; Brinson, B. E.; Smalley, R. E.; Margrave, J. L., & Hauge, R. H. (2001). Purification and Characterization of Single-Wall Carbon Nanotubes. *The Journal of Physical Chemistry B*, Vol. 105, No. 35, pp. (1157-1161), ISSN 1520-6106

Cialla, D.; Deckert-Gaudig, T.; Budich, C.; Laue, M.; Moller, R.; Naumann, D.; Deckert, V. & Popp, J. (2009). Raman to the limit: tip-enhanced Raman spectroscopic investigations of a single tobacco mosaic virus. *Journal of Raman Spectroscopy,* Vol. 40, No. 3, pp. (240-243), ISSN 0377-0486

Downes, A.; Salter, D. & Elfick A. (2006). Heating effects in tip-enhanced optical microscopy. *Optics Express*, Vol. 14, No. 12, pp.(5216-5222), ISSN 1094-4087

Downes, A.; Salter, D. & Elfick, A. (2008). Simulations of tip-enhanced optical microscopy reveal atomic resolution. *Journal of Microscopy,* Vol. 229, No. 2, pp. (184-188), ISSN 0022−2720

Dresselhaus, M. S.; Dresselhaus, G.; Jorio, A.; Souza, F. A. G. & Saito R. (2002). Raman spectroscopy on isolated single wall carbon nanotubes. *Carbon*, Vol. 40, No. 12, pp. (2043-2061), ISSN 0008-6223

Dresselhaus, M. S.; Dresselhaus, G.; R. Saito and A. Jorio (2005). Raman Spectroscopy of Carbon Nanotubes. *Physics Reports,* Vol. 409, No. 2pp.(47-99), ISSN 0370-1573

Eklund, P. C.; Holden, J. M. & Jishi, R. A. (1995). Vibrational Modes of Carbon Nanotubes; Spectroscopy and Theory. *Carbon*, Vol. 33, No. 7, pp.(959–972), ISSN 0008-6223

Frank, S.; Poncharal, P.; Wang, Z. L. & Heer, W. A. (1998). Carbon Nanotube Quantum Resistors. *Science*, Vol. 280, No. 5370, pp. (1744-1746), ISSN 0036-8075

Frey, H. G.; Keilmann, F.; Kriele, A. & Guckenberger, R. (2002). Enhancing the resolution of scanning near-field optical microscopy by a metal tip grown on an aperture probe. *Applied Physics Letters,* Vol. 81, No. 26, pp. (5030-5032), ISSN 0003-6951

Gennaro, P.; Marc, C. & Razvigor, O. (2009). High resolution probing of multi wall carbon nanotubes by tip enhanced Raman spectroscopy in gap-mode. *Chemical Physics Letters,* Vol. 469, No. 1-3, pp.(161-165), ISSN 0009-2614

Georgi, C.; Hecker, M. & Zschech, E. (2007). Raman intensity enhancement in silicon-on-insulator substrates by laser deflection at atomic force microscopy tips and particles. *Applied Physics Letters*, Vol. 90, No. 17, pp.(171102-1 - 171102-3), ISSN 0003-6951

Guan, L. (2006) Filling of Carbon Nanotube: Studies on Structure and Properties of Materials Confined in Nanospace. Peking University, Beijing

Gucciardi, P. G.; Lopes, M.; Deturche, R.; Julien, C.; Barchiesi, D. & de la Chapelle, M. L. (2008). Light depolarization induced by metallic tips in apertureless near-field optical microscopy and tip-enhanced Raman spectroscopy. *Nanotechnology*, Vol. 19, No. 21, pp.(215702), ISSN 0957-4484

Hartschuh, A. & Novotny, L. (2002). Near-field Raman spectroscopy using a sharp metal tip. *Technical Digest. Summaries of papers presented at the Quantum Electronics and Laser Science Conference,* Conference Edition (IEEE Cat. No.02CH37338),: vol.1|(271+40 suppl.) pp. (39-40), ISBN 1-55752-708-3

Hartschuh, A.; Sánchez, E. J.; Xie, X. S. & Novotny, L. (2003). High-Resolution Near-Field Raman Microscopy of Single-Walled Carbon Nanotubes. *Physical Review Letters,* Vol. 90, No. 9, pp. (095503-1-095503-4), ISSN 0031-9007

Hartschuh A., Qian H. H., Meixner A. J., Anderson N., & Novotny L. (2005). Nanoscale optical imaging of excitons in single-walled carbon nanotubes. *Nano Letters,* Vol. 5, No. 11, pp. (2310-2313), ISSN 1530-6984

Hayazawa, N.; Inouye, Y.; Sekkat, Z. & Kawata, S. (2000). Metallized tip amplification of near-field Raman scattering. *Optics Communications,* Vol. 183, No. 1-4, (September 2000), pp. (333-336), ISSN 0030-4018

Hayazawa, N.; Inouye, Y.; Sekkat, Z. & Kawata, S. (2001). Near-field Raman scattering enhanced by a metallized tip. *Chemical Physics Letters,* Vol. 335, No. 5-6, pp. (369-374), ISSN 0009-2614

Hayazawa, N.; Yano, T.; Watanabe, H.; Inouye, Y. & Kawata, S. (2003). Detection of an individual single-wall carbon nanotube by tip-enhanced near-field Raman spectroscopy. *Chemical Physics Letters,* Vol. 376, No. 1-2, pp. (174-180), ISSN 0009-2614

Hayazawa, N.; Saito, Y. & Kawata, S. (2004). Detection and characterization of longitudinal field for tip-enhanced Raman spectroscopy. *Applied Physics Letters,* Vol. 85, No., 25, pp. (6239-6241), ISSN 0003-6951

Hayazawa, N.; Watanabe, H.; Saito, Y. & Kawata, S. (2006). Towards atomic site-selective sensitivity in tip-enhanced Raman spectroscopy. *Journal of Chemical Physics,* Vol. 125, No. 24, pp. (244706), ISSN 0021-960

Iijima, S. (1991). Helical microtubules of graphitic carbon. *Nature,* Vol. 354, No. 6348, pp. (56-58), ISSN 0028-0836

Johnson, P.B. & Christy, R.W. (1972). Optical Constants of the Noble Metals. *Phys. Rev. B,* Vol. 6, No. 12, pp. (4370-4379), ISSN 1098-0121

Kalkbrenner, T.; Ramstein, M.; Mlynek, J. & Sandoghdar, V. (2001). A single gold particle as a probe for apertureless scanning near-field optical microscopy. *Journal of Microscopy-Oxford,* Vol. 202, pp. (72-76), ISSN 0022-2720

Kerker, M.; Wang, D. S. & Chew, H. (1980). Surface enhanced raman-scattering (SERS) by molecules adsorbed at spherical-particles. *Applied Optics,* Vol. 19, No. 24, pp. (4159-4174), ISSN 0003-6935

Kharintsev, S. S.; Hoffmann, G. G.; Dorozhkin, P. S.; With, G. de & Loos, J. (2007). Atomic force and shear force based tip-enhanced Raman spectroscopy and imaging. *Nanotechnology,* Vol. 18, No. 31, pp. (315502-9pp), ISSN 0957-4484

Krug, J. T. ; Sanchez, E. J. & Xie, X. S. (2002). Design of near-field optical probes with optimal field enhancement by finite difference time domain electromagnetic simulation. *Journal of Chemical Physics,* Vol. 116, No. 24, pp. (10895-10901), ISSN 0021-9606

Lee, N.; Hartschuh, R. D.; Mehtani, D.; Kisliuk, A.; Maguire, J. F.; Green, M.; Foster, M. D. & Sokolov, A. P. (2007). High contrast scanning nano-Raman spectroscopy of silicon. *Journal of Raman Spectroscopy,* Vol. 38, No. 6, pp. (789-796), ISSN 0377-0486

Li, H.; Feng, L.; Guan, L.; Shi, Z. & Gu, Z. (2004). Synthesis and purification of single-walled carbon nanotubes in the cottonlike soot. *Solid State Communications,* Vol. 132, No. 3-4, pp. (219-224), ISSN 0038-1098

Martin, O. J. F. & Girard, C. (1997). Controlling and tuning strong optical field gradients at a local probe microscope tip apex. *Applied Physics Letters,* Vol. 70, No. 6, pp. (705-707), ISSN 0003-6951

Mehtani, D.; Lee, N.; Hartschuh, R. D.; Kisliuk, A.; Foster, M. D.; Sokolov, A. P. & Maguire, J. F. (2005). Nano-Raman spectroscopy with side-illumination optics. *Journal of Raman Spectroscopy,* Vol. 36, No. 11, pp. (1068-1075), ISSN 0377-0486

Neacsu, C. C.; Steudle, G. A. & Raschko, M. B. (2005). Plasmonic light scattering from nanoscopic metal tips. *Applied Physics B-Lasers and Optics,* Vol. 80, No. 3, pp. (295-300), ISSN 0946- 2171

Novotny, L.; Bian, R. X. & Xie, X. S. (1997). Theory of nanometric optical tweezers. *Physical Review Letters,* Vol. 79, No. 4, pp. (645-648), ISSN 0031-9007

Novotny, L. (2008). Nano-optics - Optical antennas tuned to pitch. *Nature,* Vol. 455, No. n.d., pp. (887-887), ISSN 0028-0836

Otto, A. (2002). What is observed in single molecule SERS, and why?. *Journal of Raman Spectroscopy,* Vol. 33, No. 8, pp. (593-598), ISSN 0377-0486

Pettinger, B.; Picardi, G.; Schuster, R. & Ertl, G. (2000). Surface Enhanced Raman Spectroscopy: Towards single molecule spectroscopy. *Electrochemistry*, Vol. 68, pp. (942-949), ISSN 0021-891X

Pettinger, B.; Picardi, G.; Schuster, R. & Ertl G. (2002). Surface-enhanced and STM-tip-enhanced Raman spectroscopy at metal surfaces. *Single Molecules,* Vol. 3, No. 5-6, pp. (285-294), ISSN 1438-5163

Pettinger, B.; Ren, B.; Picardi, G.; Schuster, R. & Ertl, G. (2004). Nanoscale Probing of Adsorbed Species by Tip-Enhanced Raman Spectroscopy. *Physical Review Letters*, Vol. 92, No. 9, pp. (0961011- 0961014), ISSN 0031-9007

Pettinger, B.; Ren, B.; Picardi, G.; Schuster, R. & Ertl, G. (2005). Tip-enhanced Raman spectroscopy (TERS) of malachite green isothiocyanate at Au(111): bleaching behavior under the influence of high electromagnetic fields. *Journal of Raman Spectroscopy,* Vol. 36, No. 6-7, pp. (541-550), ISSN 0377-0486

Qian, H.; Gokus, T.; Anderson, N.; Novotny, L.; Meixner, A. J. & Hartschuh, A. (2006). Near-field imaging and spectroscopy of electronic states in single-walled carbon nanotubes. *Physica Status Solidi (B),* Vol. 243, No. 13, pp. (3146-3150), ISSN 0370-1972

Qian, H.; Georgi, C.; Anderson, N.; Green, A. A.; Hersam, M. C.; Novotny, L. & Hartschuh, A. (2008). Exciton transfer and propagation in carbon nanotubes studied by near-field optical microscopy. *Physica Status Solidi B*, Vol. 245, No. 10, pp. (2243-2246), ISSN 0377-0486

Rao, A. M.; Richter, E.; Bandow, S.; Chase, B.; Eklund P. C.; Williams, K. A.; Fang, S.; Subbaswamy, K. R.; Menon, M.; Thess, A.; Smalley, R. E.; Dresselhaus, G. & Dresselhaus, M. S. (1997). Diameter-Selective Raman Scattering from Vibrational Modes in Carbon Nanotubes. Science, Vol. 275, No. 5297, pp. (187-191), ISSN 0036-8075

Rao, A. M.; Chen, J.; Richter, E.; Schlecht, U.; Eklund, P. C.; Haddon, R. C.; Venkateswaran, U. D.; Kwon, Y. K. & Tománek, D. (2001). Effect of van der Waals Interactions on the Raman Modes in SingleWalled Carbon Nanotubes. *Physical Review Letters*, Vol. 86, No. 17, pp.(3895-3898), ISSN 0031-9007

Ren, B.; Picardi, G. & Pettinger, B. (2004). Preparation of gold tips suitable for tip-enhanced Raman spectroscopy and light emission by electrochemical etching. *Review of Scientific Instruments,* Vol. 75, No. 4, pp. (837-841), ISSN 0034-6748

Ren, B.; Picardi, G.; Pettinger, B.; Schuster, R. & Ertl, G. (2005). Tip-enhanced Raman spectroscopy of benzenethiol adsorbed on Au and Pt single-crystal surfaces. *Angewandte Chemie-International Edition,* Vol. 44, pp. (139-142), ISSN 1433-7851

Sackrow, M.; Stanciu, C.; Andreas, M. Lieb & Meixner A. J. (2008). Imaging Nanometre-Sized Hot Spots on Smooth Au Films with High-Resolution Tip-Enhanced Luminescence and Raman Near-Field Optical Microscopy. *Chem. Phys. Chem.,* Vol. 9, No. 2, pp. (316-320), ISSN 1439-4235

Saito, Y.; Wang, J. J.; Smith, D. A. & Batchelder, D. N. (2002). A simple chemical method for the preparation of silver surfaces for efficient SERS. *Langmuir,* Vol. 18, No. 8, pp. (2959-2961), ISSN 0743-7463

Saito, Y.; Hayazawa, N.; Kataura, H.; Murakami, T.; Tsukagoshi, K.; Inouye, Y. & Kawata, S. (2005). Polarization measurements in tip-enhanced Raman spectroscopy applied to single-walled carbon nanotubes. *Chemical Physics Letters,* Vol. 410, No. 1-3, pp. (136-141), ISSN 0009-2614

Saito, Y.; Motohashi, M.; Hayazawa, N. & Kawata, S. (2008). Stress imagining of semiconductor surface by tip-enhanced Raman spectroscopy. *Journal of Microscopy,* Vol. 229, No. n.d., pp. (217-222), ISSN 0022-2720

Schmid, T.; Yeo, B. S.; Zhang, W. & Zenobi, R. (2007). Name of paper Use of tip-enhanced vibrational spectroscopy for analytical applications in chemistry, biology, and materials science. In: Kawata S, V. M. Shalaev, ed. Tip enhancement. Oxford: Elsevier, pp. (115-155), ISSN 1871-0018

Steidtner, J. & Pettinger, B. (2007). High-resolution microscope for tip-enhanced optical processes in ultrahigh vacuum. *Review of Scientific Instruments,* Vol. 78, No. 103104, pp. (1-8), ISSN 0034-6748

Steidtner, J. & Pettinger, B. (2008). Tip-enhanced Raman spectroscopy and microscopy on single dye molecules with 15 nm resolution. *Physical Review Letters,* Vol. 100, No. 23, pp. (236101-1-236101-4), ISSN 0031-9007

Stöckle, M.; Doug, S. Y.; Deckert, V. & Zenobi, R. (2000). Nanoscale chemical analysis by tip-enhanced Raman spectroscopy. *Chemical Physics Letters,* Vol. 318, pp. (131-136), ISSN 0009-2614

Sun, W. X & Shen, Z X. (2001). A practical nanoscopic Raman imaging technique realized by near-field enhancement. *Materials Physics and Mechanics,* Vol. 4, No. 1, pp. (17-21), ISSN 1605-8119

Sun, W. X. & Shen, Z. X. (2003). Near-field scanning Raman microscopy using apertureless probes. *Journal of Raman Spectroscopy,* Vol. 34, No. 9, pp. (668-676), ISSN 0377-0486

Tarun, A.; Hayazawa, N. & Kawata, S. (2009). Tip-enhanced Raman spectroscopy for nanoscale strain characterization. *Analytical and Bioanalytical Chemistry,* Vol. 394, pp. (1775–1785), ISSN 1618-2642

Wang, J. J.; Saito, Y.; Batchelder, D. N.; Kirkham, J.; Robinson, C. & Smith, D. A. (2005). Controllable method for the preparation of metalized probes for efficient scanning near-field optical Raman microscopy. *Applied Physics Letters,* Vol. 86, No. 26, pp. (2631111 - 2631113), ISSN 0003-6951

Wang, R.; Wang, J.; Hao, F.; Zhang, M. & Tian, Q. (2010a). Tip-enhanced Raman spectroscopy with silver-coated optical fiber probe in reflection mode for investigating multiwall carbon nanotubes. *Applied Optics,* Vol. 49, No. 10, pp. (1845-1848), ISSN 1559-128X

Wang, R. (2010b). Research on the Tip-Enhanced Raman Spectroscopy in Reflection Mode Based on Silver-Coated Optical Fiber Probe, Tsinghua University, Beijing, China

Wang, R.; Hao, F.; Zhang, M.; Wang, J.; Yu, J. & Tian, Q. (2010c). Tip-Enhanced Raman Spectroscopy and System Design. *Laser & Optoelectronics Progress*, Vol. 47, No. n.d., pp. (031601-1-031601-10), ISSN 1006-4125

Watanabe, H.; Hayazawa, N.; Inouye, Y. & Kawata, S. (2005). DFT vibrational calculations of Rhodamine 6G adsorbed on silver: Analysis of tip-enhanced Raman spectroscopy. *Journal of Physical Chemistry B,* Vol. 109, No. 11, pp. (5012-5020), ISSN 1520-6106

Watanabe, H.; Ishida, Y.; Hayazawa, N.; Inouye, Y. & Kawata, S. (2004). Tip-enhanced near-field Raman analysis of tip-pressurized adenine molecule. *Physical Review B,* Vol. 69, No. 15, pp. (15541801-15541811), ISSN 1098-0121

Watanabe, H.; Ishida, Y.; Hayazawa, N.; Inouye, Y. & Kawata, S. (2004).Tip-enhanced near-field Raman analysis of tip-pressurized adenine molecule. *Physical Review B*, Vol. 69, No. 15, pp.(155418-1- 155418-11), ISSN 1098-0121

Wei, J. Q.; Zhu, H. W.; Li, Y. H.; Chen, B.; Jia, Y.; Wang, K.; Wang, Z.; Liu, W.; Luo, J.; Zheng, M.; Wu, D.; Zhu, Y. & Wei, B. (2006). Ultrathin Single-Layered Membranes from Double-Walled Carbon Nanotubes. *Advanced Materials,* Vol. 18, No. 13, pp. (1695-1700), ISSN 0935-9648

Wu, X.; Wang, J. , Wang R. , Xu J. , Tian Q. & Yu J.(2009). Detection of Single-Walled Carbon Nanotube Bundles by Tip-Enhanced Raman Spectroscopy. Spectroscopy and Spectral Analysis, Vol. 29, No. 10 ,pp2681-2685, ISSN 1000-0593

Wu, X.; Zhang, M.; Wang, J. & Tian, Q. (2010). Experimental Research on Double-walled Carbon Nanotubes using Tip-enhanced Raman Spectroscopy. *Journal of the Korean Physical Society*, Vol. 56, No. 4, pp.(1103-1108), ISSN 0374-4884

Yano, T.; Verma, P. & Kawata S. (2006). Diameter-selective near-field Raman analysis and imaging of isolated carbon nanotube bundles. *Applied Physics Letters*, Vol. 88, No. 9, pp.(093125), ISSN 0003-6951

Yano, T.; Verma, P.; Saito, Y.; Ichimura, T. & Kawata, S. (2009). Pressure-assisted tip-enhanced Raman imaging at a resolution of a few nanometers, *Nature Photonics*, Vol. 3, No. 8, pp.(473-477), ISSN 1749-4885

Yeo, B. S.; Zhang, W. H.; Vannier, C. & Zenobi, R. (2006). Enhancement of Raman signals with silver-coated tips. *Applied Spectroscopy*, Vol. 60, No. 10, pp.(1142-1147), ISSN 0003-7028

Yu, M. F.; Files, B. S.; Arepalli, S. & Ruoff, R. S. (2000). Tensile Loading of Ropes of Single Wall Carbon Nanotubes and their Mechanical Properties. *Physical Review Letters*, Vol. 84, No. 24 , pp. (5552-5555), ISSN 0031-9007

Zhang, D.; Wang, X.; Braun, K.; Egelhaaf, H. J.; Fleischer, M.; Hennemann, L.; Hintz, H.; Stanciu, C.; Brabec, C. J.; Kern, D. P. & Meixner, A. J. (2009). Parabolic mirror-assisted tip-enhanced spectroscopic imaging for non-transparent materials. *Journal of Raman Spectroscopy,* Vol. 40, No. 10, pp. (1371–1376), ISSN 0377-0486

Zhang, W. H.; Yeo, B. S.; Schmid, T. & Zenobi, R. (2007). Single molecule tip-enhanced Raman spectroscopy with silver tips. *Journal of Physical Chemistry,* Vol. 111, No. 4, pp. (1733-1738), ISSN 1520-6106

Zhu, L.; Atesang, J.; Dudek, P.; Hecker, M.; Rinderknecht, J.; Ritz, Y.; Geisler, H.; Herr, U.; Greer, R. & Zschech, E. (2007a). Experimental challenges for approaching local strain determination in silicon by nano-Raman spectroscopy. *Materials Science-Poland*, Vol. 25, No. 1, pp.(19-31), ISSN 0137–1339

Zhu, L.; Georgi, C.; Hecker, M.; Rinderknecht, J.; Mai, A.; Ritz, Y. & Zschech, E. (2007b). Nano-Raman spectroscopy with metallized atomic force microscopy tips on strained silicon structures. *Journal of Applied Physics*, Vol. 101, No. 10, pp.(104305-1-104305-6), ISSN 0021-8979

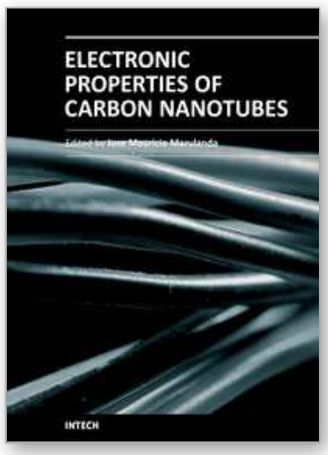

Electronic Properties of Carbon Nanotubes

Edited by Prof. Jose Mauricio Marulanda

ISBN 978-953-307-499-3
Hard cover, 680 pages
Publisher InTech
Published online 27, July, 2011
Published in print edition July, 2011

Carbon nanotubes (CNTs), discovered in 1991, have been a subject of intensive research for a wide range of applications. These one-dimensional (1D) graphene sheets rolled into a tubular form have been the target of many researchers around the world. This book concentrates on the semiconductor physics of carbon nanotubes, it brings unique insight into the phenomena encountered in the electronic structure when operating with carbon nanotubes. This book also presents to reader useful information on the fabrication and applications of these outstanding materials. The main objective of this book is to give in-depth understanding of the physics and electronic structure of carbon nanotubes. Readers of this book should have a strong background on physical electronics and semiconductor device physics. This book first discusses fabrication techniques followed by an analysis on the physical properties of carbon nanotubes, including density of states and electronic structures. Ultimately, the book pursues a significant amount of work in the industry applications of carbon nanotubes.

How to reference

In order to correctly reference this scholarly work, feel free to copy and paste the following:

Jia Wang, Xiaobin Wu, Rui Wang and Mingqian Zhang (2011). Detection of Carbon Nanotubes using Tip-Enhanced Raman Spectroscopy, Electronic Properties of Carbon Nanotubes, Prof. Jose Mauricio Marulanda (Ed.), ISBN: 978-953-307-499-3, InTech, Available from: http://www.intechopen.com/books/electronic-properties-of-carbon-nanotubes/detection-of-carbon-nanotubes-using-tip-enhanced-raman-spectroscopy

INTECH
open science | open minds

InTech Europe
University Campus STeP Ri
Slavka Krautzeka 83/A
51000 Rijeka, Croatia
Phone: +385 (51) 770 447
Fax: +385 (51) 686 166
www.intechopen.com

InTech China
Unit 405, Office Block, Hotel Equatorial Shanghai
No.65, Yan An Road (West), Shanghai, 200040, China
中国上海市延安西路65号上海国际贵都大饭店办公楼405单元
Phone: +86-21-62489820
Fax: +86-21-62489821

IntechOpen